Climate Dynamics (2020) 55:131–151
https://doi.org/10.1007/s00382-018-4368-z

The diurnal cycle of East Asian summer monsoon precipitation simulated by the Met Office Unified Model at convection-permitting scales

Puxi Li[1,2] · Kalli Furtado[3] · Tianjun Zhou[1,2] · Haoming Chen[4] · Jian Li[4] · Zhun Guo[1,6] · Chan Xiao[5]

Received: 7 February 2018 / Accepted: 10 July 2018 / Published online: 27 July 2018

Abstract
A limited area convection permitting model (CPM) based on the Met Office Unified Model, with a 0.04° (4.4 km) horizontal grid spacing, is used to simulate an entire warm-season of the East Asian monsoon (from April to September 2009). The simulations are compared to rain gauge observations, reanalysis and to a lower resolution regional model with a 0.12° (13.2 km) grid spacing that has a parametrization of subgrid-scale convective clouds and precipitation. The 13.2 km simulation underestimates precipitation intensity, produces rainfall too frequently, and shows evident biases in reproducing the diurnal cycle of precipitation and low-level wind fields. In comparison, the CPM shows significant improvements in the spatial distribution of precipitation intensity, although it overestimates the intensity magnitude and has a wet bias over central eastern China. The diurnal cycle of precipitation over Mei-yu region, southern China and the eastern periphery of the Tibetan Plateau, as well as the diurnal cycle of low-level winds over both the Mei-yu region and southern China are better simulated by the CPM. Over the Mei-yu region, in both simulations and observations, the local atmospheric instability in the afternoon is favorable for upward motion and rainfall. The CPM receives more sensible heat flux from the surface, has a stronger upward motion, and overestimates water vapor convergence based on moisture budget diagnosis. All these processes help explain the excessive late afternoon rainfall over the Mei-yu region in the CPM simulation.

Keywords Convection permitting model · Precipitation characteristics · Diurnal cycle · Moisture budget diagnosis · Water vapor transport

This paper is a contribution to the special issue on Advances in Convection-Permitting Climate Modeling, consisting of papers that focus on the evaluation, climate change assessment, and feedback processes in kilometer-scale simulations and observations. The special issue is coordinated by Christopher L. Castro, Justin R. Minder, and Andreas F. Prein.

✉ Tianjun Zhou
zhoutj@lasg.iap.ac.cn

1 LASG, Institute of Atmospheric Physics, Chinese Academy of Science, Beijing 100029, China

2 University of Chinese Academy of Sciences, Beijing 100049, China

3 Met Office, Exeter, UK

4 Chinese Academy of Meteorological Sciences, China Meteorological Administration, Beijing 100081, China

5 National Climate Center, China Meteorological Administration, Beijing, China

6 Climate Change Research Center, Institute of Atmospheric Physics, Chinese Academy of Sciences, Beijing 100029, China

1 Introduction

The diurnal cycle of precipitation is an important aspect of our weather and climate. It is closely related to surface temperature, moist convection, the formation of clouds and boundary-layer development (Dai et al. 1999; Yang and Slingo 2001). Furthermore, it is intimately connected with both regional and synoptic-scale dynamical and thermal conditions and thus provides a good test bed for weather and climate models (Dai and Trenberth 2004). On a global scale, the diurnal variations of precipitation are evident over much of the world's land and oceans, especially during the summer months. For example, there is a substantial nocturnal-precipitation maximum over the oceans, due to cloud-radiative interactions, the diurnal circulation between land and ocean (Dai and Deser 1999) and the evolution of deep convective systems, and a late-afternoon maximum of showery precipitation over most areas of land, due to solar heating on the ground (Dai 2001, 2006; Dai et al. 2007;

Dai and Trenberth 2004). The diurnal cycle of precipitation associated with the East Asian summer monsoon (EASM) shows unique features due to complex interactions between surface heating, orography and the monsoon flow (Yu et al. 2004, 2007a, b). The observed warm-season precipitation over contiguous China has distinct diurnal variations with considerable regional features (Yu et al. 2007a, b, 2009; Zhou et al. 2008; Yuan et al. 2010, 2012; Li 2017). Over inland areas of southern China, the summer rainfall peaks in the late afternoon (i.e., between 3 p.m. and 7 p.m., local solar time (LST), hereafter 1500 LST and 2000 LST; Yu et al. 2007a, b; Zhou et al. 2008; Jiang et al. 2017). On the eastern periphery of the Tibetan Plateau (TP), there is a large contribution from nocturnal rainfall (between 2200 LST and 0300 LST; Yu et al. 2007b; Zhou et al. 2008; Chen et al. 2010a). Along the Yangtze River valley, the geographical distribution of diurnal-cycle variation exhibits an eastward phase delayed in the timing of peak precipitation (Asai et al. 1998; Yu et al. 2007a, b; Chen et al. 2010a).

The diurnal cycle of precipitation in monsoon regions has been a rigorous test-bed for validating cumulus and other parametrizations in numerical models. Current state-of-the-art climate models generally show poor performance in reproducing the diurnal cycle (Dai 2006; Flato et al. 2013; Yuan et al. 2013; Covey et al. 2016). Moreover, most general circulation models (GCMs) and regional circulation models (RCMs) are highly sensitive to cloud microphysics, boundary-layer, land-surface physics and cumulus-parametrization schemes (Dai et al. 1999; Liang et al. 2004; Chen et al. 2010b; Zhang and Chen 2016). In particular, the cumulus-parameterization has been regarded as the single largest source of uncertainty in precipitation simulation (Dai et al. 1999; Liang et al. 2004; Dai 2006; Brockhaus et al. 2008; Bukovsky and Karoly 2009; Hohenegger et al. 2009; Sun et al. 2016; Zhang and Chen 2016). Many long-standing model biases are related to the convection schemes, such as excessive light rainfall and too little heavy rainfall, errors in the timing of afternoon precipitation over land, and an inability to produce meso-scale convective systems (Yang and Slingo 2001; Dai 2006; Guichard et al. 2010; Stephens et al. 2010; Birch et al. 2014).

Due to advances in scientific computing, numerical meshes can now be refined to the point where the parametrization of convection can be switched off for many climate and climate-change applications (Prein et al. 2015). When the horizontal grid spacing is 4 km or less (Weisman et al. 1997), it becomes realistically possible to run RCMs with "explicit" convection. Such models are usually called "convection-permitting" models (CPMs), or "convection-resolving" models, and presumably have a better representation of small-scale physical processes, such as those due to moist-processes, complex terrain and land–atmosphere coupling, than coarser RCMs. CPMs show improvements in the simulation of the diurnal cycle of precipitation and the representation of convection (Guichard et al. 2004; Pearson et al. 2013; Ban et al. 2014; Prein et al. 2017a). Improvements are also evident in the simulation of precipitation frequency, intensity and precipitation histograms (Dai et al. 2017), both light and extremely heavy precipitation (Li et al. 2012), the Madden–Julian oscillation (Miura et al. 2007; Benedict and Randall 2009; Sato et al. 2009), and even the doldrums over tropical Atlantic (Klocke et al. 2017). CPM is useful for providing improved projections of future changes in hourly precipitation extremes (Kooperman et al. 2013; Fosser et al. 2015, 2017; Kendon et al. 2014; Liu et al. 2017; Prein et al. 2017b, c) and changes in precipitation histograms (Dai et al. 2017). One major weakness of CPMs is the overestimation of rainfall amount over certain regions (Weisman et al. 1997; Holloway et al. 2012; Birch et al. 2014), but that was not an issue over North America (Dai et al. 2017; Liu et al. 2017).

CPMs have been demonstrated that they are useful tools in regional climate modeling and projection. A present-day and future climate simulations using a CPM with a horizontal grid-spacing of 2.2 km over the Alps showed that both extreme day-long and hour-long precipitation events intensified with temperature as constrained by the Clausius–Clapeyron relation, along with a better simulation of the precipitation diurnal cycle (Ban et al. 2014, 2015). A continental-scale CPM simulation of the West African monsoon (WAM) shows better simulations of storm structures, and the diurnal cycle of rainfall intensity (Marsham et al. 2013). Stein et al. (2015) studied the effect of reducing model-grid spacing to 4 or 1.5 km over WAM region, and validated model cloud structures against satellite retrievals from CloudSat. They found that, compared with simulations using a coarser-resolution regional model, the CPM showed improvements in the representation of thin-anvil cirrus and mid-level clouds. In addition, the accurate representation of the diurnal cycle of convection and the ability to trigger convection is key to improving the model performance over the WAM (Birch et al. 2014). The diurnal cycle of precipitation over the maritime continent is improved when the grid-resolution is increased from 12 to 4 km (Birch et al. 2016). CPM simulations of the present and future climates over North America have also been done and found to produce realistic characteristics of convection and precipitation (Dai et al. 2017; Liu et al. 2017; Prein et al. 2017a).

The monsoon rainfall over East Asia is a useful test bed for climate modeling. But the performances of limited area CPMs in simulating precipitation diurnal cycle remain unknown. In this study, we aim to: (1) evaluate the performance of a limited area CPM in reproducing the diurnal cycles of precipitation frequency, intensity and amount, and their geographical distribution over East Asia and understand what aspects or factors are improved in a CPM, over a low-resolution version of the same model with parametrized

convection; (2) quantify the model performance in reproducing the diurnal cycle of large-scale circulation associated with diurnal variations of precipitation.

The remainder of this paper is organized as follows. The model and experiment design, description of the observation and reanalysis datasets, and analysis methods are described in Sect. 2. In Sect. 3, we evaluate the performance of the two high resolution regional model simulations in reproducing the summer mean precipitation characteristics, and investigate how well the CPM simulates the diurnal cycle of precipitation and the associated large scale circulation compared to a convection-parametrized model. Finally, a summary and a discussion are given in Sect. 4.

2 Methodology

2.1 Model and experiment design

Two season-long simulations were performed using regional configurations of the Met Office Unified Model (MetUM; Cullen 1993; Brown et al. 2012): a convection-permitting version with an angular grid spacing of 0.04° (corresponding to approximately 4.4 km, in the model's rotated-pole coordinate system) and a 20-s time step; a lower-resolution (convection-parameterized) simulation, with a grid spacing of 0.12° (13.2 km) and a 60-s time step. Both simulations have the spatial domain shown in Fig. 1 (big blue box). The overall configuration of the convection-permitting model is similar to that described in Pearson et al. (2010) and Lean et al. (2008), who tested the implications for convection over the United Kingdom. The regional configuration used the Met Office Global Atmosphere version 6.1 (GA6.1; Walters et al. 2017), which (at the time of running) was the version of the Unified Model used operationally by the Met Office for global weather and climate prediction. The domains for both simulations were identical (Fig. 1). Since the continental CPM simulation is computationally very expensive, we performed simulations that cover the warm seasons of 2009, which is regarded as a normal monsoon year. The duration of the simulations was from 1st April to 30th September in 2009. Further details of the model grids are summarized in Table 1.

In the convection-parametrized (13.2 km) simulation, the convection scheme is based on the Gregory–Rowntree scheme (Gregory and Rowntree 1990) with closure based on the convective available potential energy (CAPE)

Table 1 Summary of the different horizontal resolution model simulations used in the studies

Resolution (Km)	N_x	N_y	$\Delta_{x,\ y}$ (°)	Lon_0	Lat_0
13.2	432	208	0.12	284.22	57.54
4.4	1296	624	0.04	284.22	57.54

$N_{x,y}$ are the number of grid boxes in the relevant directions, $\Delta_{x,\ y}$ is the grid spacing and Lon_0 and Lat_0 are the pole longitude and pole latitude in the rotated system

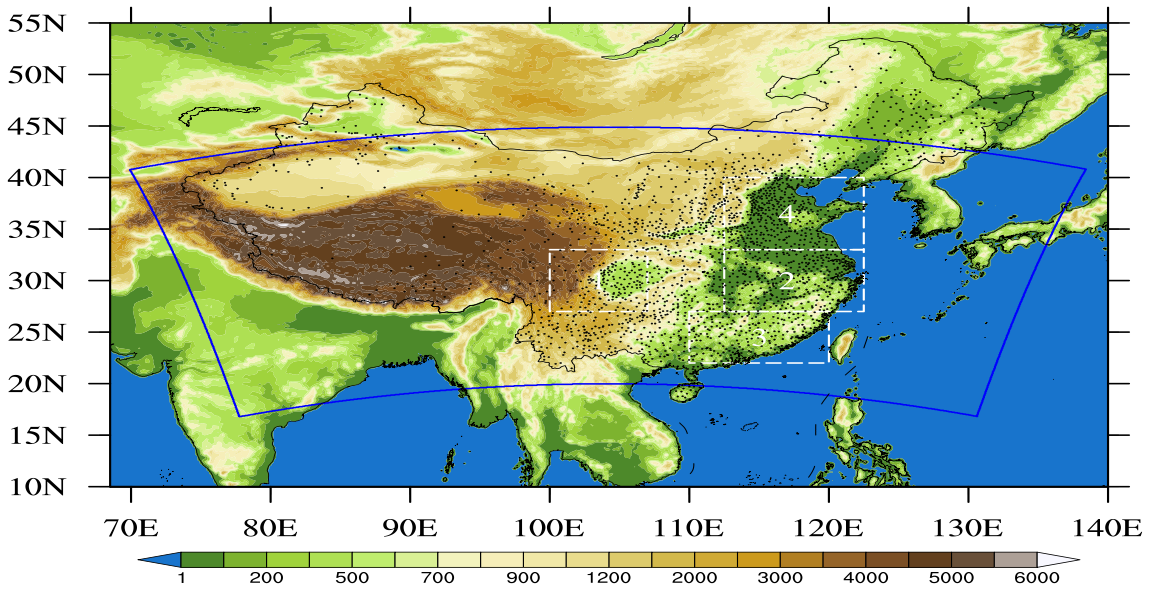

Fig. 1 Surface elevation (shaded, units: m) and location (black dots) of the 2420 national rain gauge stations over China, four sub-regions (rectangles; Region 1: upper Yangtze River valley; Region 2: Mei-yu region; Region 3: southern China; Region 4: area between Yangtze River and Yellow River) are shown here for regional averaging. The big blue box indicates the integration domain used in the convection-permitting simulation (4.4 km) and convection-parametrized simulation (13.2 km)

and a relaxation timescale of 30 min. In the convection-permitting simulation, "explicit" convection was achieved by increasing the closure time scale of the parametrized convection for high CAPE, such that the parameterization of deep convection is effectively switched off. The parameterization of shallow cumulus, which is basically the same as Gregory–Rowntree scheme, with some modifications following Grant et al. (2001), is active in both two simulations.

The regional models derive their lateral-boundary conditions hourly from a global-model simulation using the GA6.1 configuration with a resolution of 0.2°. We use the analyses provided by the European Centre for Medium-Range Weather Forecast (ECMWF) to re-initialize the global driving-model on a six-hourly forecast cycle, thus constraining the nested simulations to be reasonably close to the re-analyzed atmospheric state. The sea surface temperature (SST) is updated daily from Operational Sea Surface Temperature and Sea Ice Analysis (OSTIA; Donlon et al. 2012). The model uses a terrain-following hybrid height coordinate (η), which is described in detail in Davies et al. (2005).

2.2 Description of the observation and reanalysis datasets

Surface hourly rain gauge data from 2420 stations in 2009 are used in this study, which were obtained from the National Meteorological Information Center (NMIC) of the China Meteorological Administration (Zhang et al. 2016). Most of the stations are located in eastern China where the distribution is relatively dense (Fig. 1). The precipitation measurements were made by siphon or tipping-bucket rain gauges and were collected automatically by computers. The data has been quality controlled by NMIC (Zhang et al. 2016). Given that annual precipitation over most of China occurs mainly between June and August (JJA; Zhou and Yu 2005; Zhou et al. 2008), and the diurnal cycle is strongest in summer (Dai et al. 2007; Zhou et al. 2008; Chen et al. 2010a), we focus on the summer season in this paper.

The Modern-Era Retrospective analysis for Research and Applications, Version 2 reanalysis datasets (MERRA2; Gelaro et al. 2017) were used to reveal the diurnal cycle of large-scale circulations. These included hourly surface latent and sensible heat flux, and three-hourly vertical velocity, zonal and meridional wind components, specific humidity, geopotential height and air temperature. The results based on MERRA2 data are broadly comparable with those from the Japanese 55-year Reanalysis Projects (JRA55; Ebita et al. 2011) and ECMWF interim reanalysis (ERA-Interim, hereafter ERAIM; Dee et al. 2011). Thus in the following section, most of the results are shown by using MERRA2 because of the high temporal and spatial resolution.

2.3 Analysis methods

Following previous studies (Dai et al. 1999; Yu and Li 2016; Chen and Dai 2018), in our analysis, the precipitation frequency (F) is defined as the percentage of all hours during the period which had measurable precipitation (> 0.1 mm h^{-1}), the precipitation intensity (I) is defined as the average precipitation rate over all the precipitating hours, and the precipitation amount (A) is defined as the accumulated precipitation amount over a given time period. We calculated the F, I, and A at each grid point during the period of June to August in 2009.

To characterize the diurnal cycle of precipitation A, F and I, we first used the hourly precipitation data over all days during the studying period to derive a composite diurnal cycle of precipitation A, F and I, then used T_{max} to denote the local solar time of the maximum in the composite diurnal cycle of precipitation A, F and I over central eastern China (97.5°E–122.5°E, 18.0°N–41.0°N).

The results of Chen and Dai (2018) show that the estimated F and I are highly sensitive to the data spatial resolution. Moreover, they highlighted the need to have similar resolutions when comparing observations and models. To enhance the comparability between the observation and our model simulations, we first averaged the station data within each convection-parametrized model grid (0.12° grid) to produce a gridded precipitation dataset, then masked out the grids which did not contain stations. We also averaged the 0.04° CPM data onto the 0.12° grid without spatial interpolation. After these procedures, we computed the precipitation F and I, and their diurnal cycles.

For observations, we further checked the differences between calculating the precipitation F and I at the original scattered 2420 rain gauge locations and from the new 0.12° observational gridded precipitation dataset (contains 2260 grid points with non-zero values), we found the estimated F and I are highly consistent (figures are not shown). For all quantitative comparisons between models and observations (such as the pattern correlation coefficients, the root mean square errors, and the diurnal cycle), we used the new gridded precipitation dataset. For visual clarity, when plotting maps of the spatial distributions of rainfall, we applied the iterative improvement objective analysis method (Cressman 1959) to fill the small gaps by using NCAR Command Language (http://www.ncl.ucar.edu/Document/Functions/Built-in/obj_anal_ic.shtml), the influencing radius array was set up to (/0.24°, 0.12°/). When comparing the differences between the model simulations and MERRA2 reanalysis, all variables that are derived from the model simulations are averaged onto the same grid as the MERRA2 reanalysis.

Based on the different underlying surface types and diurnal features, four sub-regions are defined similar to those by Zhou et al. (2008). These domains are marked in Fig. 1,

and correspond to the upper Yangtze River valley, the-lower Yangtze River valley (hereafter the "Mei-yu region"), southern China and the regions between the Yangtze River and the Yellow River. We use local solar time (LST) to study the diurnal variation of precipitation characteristics, and use Beijing Standard Time (BST) to reveal the diurnal cycle of large scale atmospheric circulation in our analysis.

The composite diurnal cycle of precipitation A, F and I over each sub-region is normalized as

$$D(h) = \frac{R(h) - \overline{R}}{\overline{R}} \tag{1}$$

where R(h) is the original, and D(h) is the rainfall after normalization by the daily mean $\overline{R}$ (Yu et al. 2007a; Yuan et al. 2013).

To understand the relationship between local atmospheric instability and the afternoon rainfall peaks, we examined the moist static energy (MSE) in both reanalysis and model simulations. The MSE is the sum of the sensible heat, latent heat and geopotential contents of a parcel:

$$MSE = c_p T + L_v q + gz \tag{2}$$

where c_p and L_v denote the specific heat of air and the latent heat of water vaporization, respectively. T is the air temperature, q is the specific humidity, g is the gravitational acceleration and z is the geopotential height. An MSE profile decreasing with altitude indicates an unstable atmosphere. MSE analysis is widely used in studying instability associated with rainfall (Pu and Cook 2012; Neupane and Cook 2013; Lau and Kim 2017). The diurnal variations in MSE are mainly contributed by the temperature ($c_p T$) and moisture components ($L_v q$), the changes of geopotential are negligible (Pu and Cook 2012; Neupane and Cook 2013), thus we mainly focus on the $c_p T$ and $L_v q$ components of the MSE changes.

To better understand the large scale circulation dominating the late afternoon rainfall (from 1400 LST to 2000 LST) over the Mei-yu region, we perform a moisture budget analysis following previous studies (Seager et al. 2010; Chou and Lan 2012; Lin et al. 2014; Ma and Zhou 2015; Li et al. 2017). The moisture budget equation is:

$$\mathrm{P} = -\partial_t \langle q \rangle - \nabla \cdot \left\langle q\vec{V} \right\rangle + \mathrm{E} + \delta \tag{3}$$

where P and E denote precipitation and evaporation, q is specific humidity and $\vec{V}$ is wind vector. δ is a residual term including transient eddies (Trenberth and Guillemot 1995; Zhou and Yu 2005), and contributions from surface processes and model interpolation bias (Seager et al. 2010; Peng and Zhou 2017). "<>" denotes a vertical mass integration through the whole troposphere (Eq. 4),

$$\langle X \rangle = \frac{1}{g} \int_{p_s}^{p_T} X dp \tag{4}$$

where g is gravitational acceleration, p_s is surface pressure and p_T is the pressure of the tropopause, taken as 100 hPa. The component of $\partial_t \langle q \rangle$ in Eq. 3 is the time derivative of vertically-integrated specific humidity, which indicates the change of local water vapor storage. $-\nabla \cdot \left\langle q\vec{V} \right\rangle$ is the convergence of integrated moisture flux. Each component on the right side of Eq. 3 is calculated by using the hourly output from regional simulation, and three-houly MERRA2 reanalysis. The 3-h variables (corresponding to the MERRA2 time interval) are then averaged to calculate the climatological summer mean late afternoon rainfall over the Mei-yu region.

3 Results

3.1 Summer mean precipitation amount, frequency and intensity

The results for the summer mean precipitation A, F and I from the rain gauges and model simulations are shown in Fig. 2. In the observations, there is an evident monsoon rainband stretching from the southwest to the northeast, with several centers located in the eastern periphery of the TP (100°E–107°E, 27°N–33°N), the coastal areas over southern China (110°E–120°E, 22°N–27°°N) and the Mei-yu region (112.5°E–122.5°E, 27°N–33°N). The convection-permitting (CPM 4p4) and convection-parametrized (hereafter, "large-scale model", LSM 13p2) simulations both show large-scale patterns that resemble the rain-gauge observations. Compared with rain gauge observation, the CPM 4p4 and LSM 13p2 have pattern correlation coefficients (PCCs) of 0.56 and 0.63, and root mean square errors (RMSEs) of 3.48 and 3.00 mm day^{-1}, respectively. The LSM 13p2 realistically simulates the magnitude of precipitation A, except that the pattern is too uniform. In the observations, the spatial distribution of precipitation A is obviously affected by the underlying surface and uneven regional distribution, but these phenomena are less pronounced in the results of LSM 13p2. In contrast, the CPM 4p4 reasonably reproduces the locations of the three rainfall centers along with an overestimation of precipitation A magnitude. The precipitation A is above 12.0 mm day^{-1} over southeastern China and the Mei-yu region in CPM 4p4, compared to 7.0–10.0 mm day^{-1} in rain-gauge data.

In the observations, the large-scale features of the JJA-mean precipitation F are similar to precipitation A. Figure 2d shows that the precipitation F is about 15% in the eastern periphery of TP, about 12% over the Mei-yu region

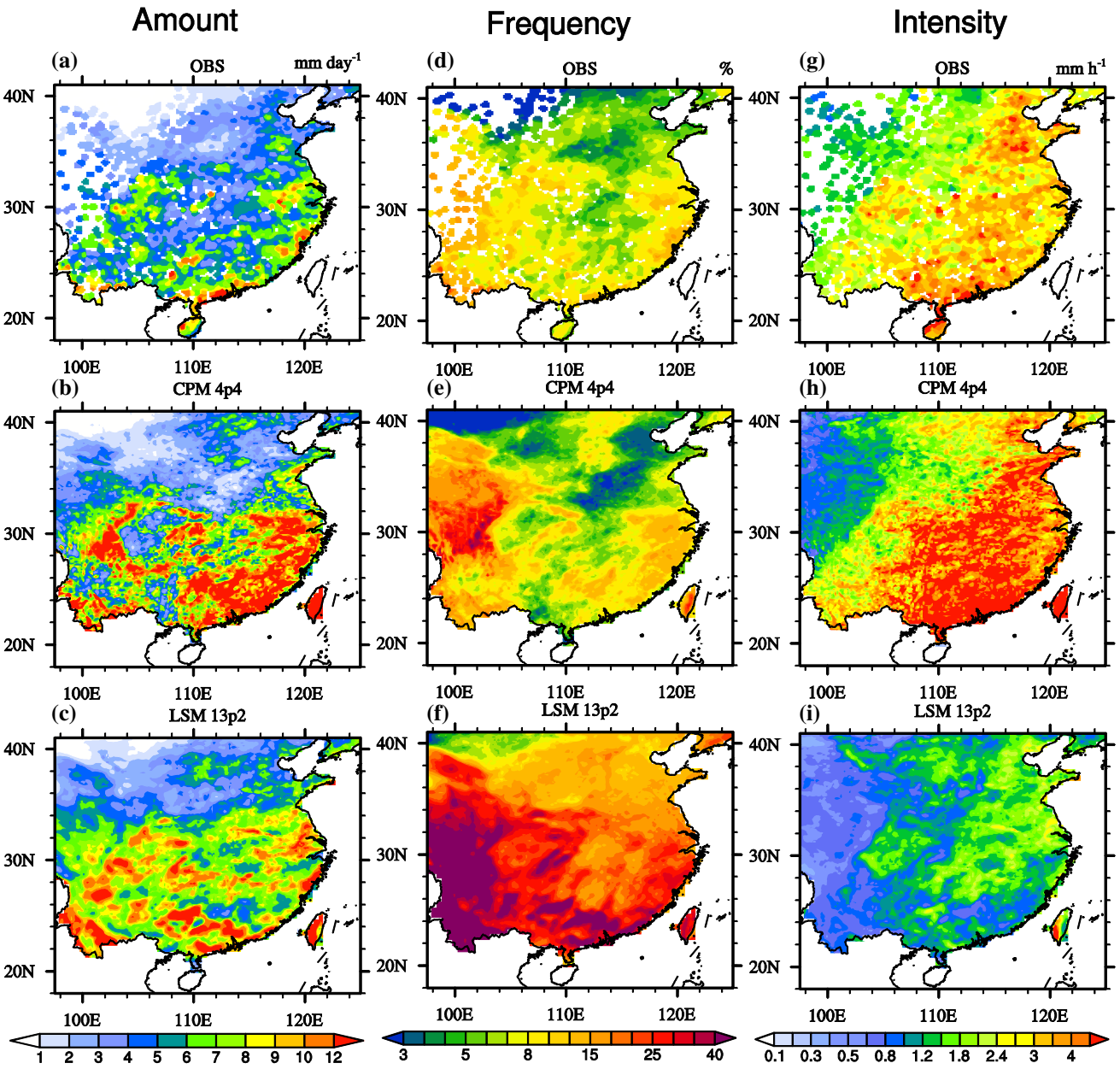

Fig. 2 Spatial distributions of summer (June–August) precipitation characteristics in 2009. **a–c** Precipitation amount (unit: mm day^{-1}); **d–f** precipitation frequency (unit: %); **g–i** precipitation intensity (unit: mm h^{-1}) from **a, d, g** 2420 rain gauge observations; **b, e, h** convection-permitting model simulations (CPM 4p4); **c, f, i** convection-parametrized model simulations (LSM 13p2)

and southeastern China in the observations. The LSM 13p2 simulation could reproduce the spatial distribution of precipitation F (with a PCC value of 0.74), but it produces too frequent rainfall, overestimates the magnitude, with a precipitation F higher than 20% over most regions (resulting in a relatively large RMSE of 19.15%; Fig. 2f). Improvements are seen in CPM 4p4 as evidenced by the three centers of precipitation F and the magnitude (with a PCC of 0.64 and a RMSE of 3.19%). One evident weakness of CPM 4p4 is the underestimation of the precipitation F over the Sichuan basin (the eastern part of region 1) and the coastal region over southern China (around 110°E, 22°N).

In rain-gauge observations, there are several local maxima in rainfall intensity over southern China (3.0–4.0 mm h^{-1}), and over the region between the Yangtze and the Yellow Rivers (112.5°E–122.5°E, 33°N–40°N). The observed south-China maximum is missing in the LSM 13p2 simulation, but it could reproduce the precipitation I center over the region between the Yangtze and the Yellow Rivers. Overall, the precipitation I was underestimated by

the LSM 13p2 over the central eastern China (with a PCC value of 0.42 and a RMSE of 1.65 mm h^{-1}). In contrast, encouraging results are seen in the CPM 4p4 simulation. The pattern of I closely resembles the rain gauge observation, with a PCC of 0.60 and a RMSE of 1.30 mm h^{-1}. The weakness of the CPM 4p4 simulation is the overestimation of the magnitude: with over 4.5 mm h^{-1} in the simulation versus about 3.5 mm h^{-1} in the rain-gauge observation over most parts of eastern China.

3.2 Diurnal cycle of precipitation amount, frequency and intensity

To identify the spatial distribution of the diurnal cycle, the LST of the maximum in the composite diurnal cycle of precipitation A, F and I are shown in Fig. 3. In rain gauge observations, the eastern periphery of the TP shows nocturnal rainfall (2100 LST to 0300 LST; Fig. 3a), which is due to concurrent peaks in both the precipitation F (Fig. 3d) and I (Fig. 3g). Southern China is dominated by the afternoon rainfall (on average the peak rainfall occurs around 1500 LST). The regions between the Yangtze and the Yellow Rivers see two peaks around 0600 LST and 1800 LST in both precipitation A and I. The observed features are poorly simulated by the LSM 13p2, including too early an afternoon peak (around 1300 LST) over eastern China (Fig. 3f), and the evident biases in reproducing the diurnal variation of precipitation A (Fig. 3c) and I (Fig. 3i). The CPM 4p4 shows superiority in the simulation of the nocturnal rainfall peak over the eastern periphery of the TP and the afternoon

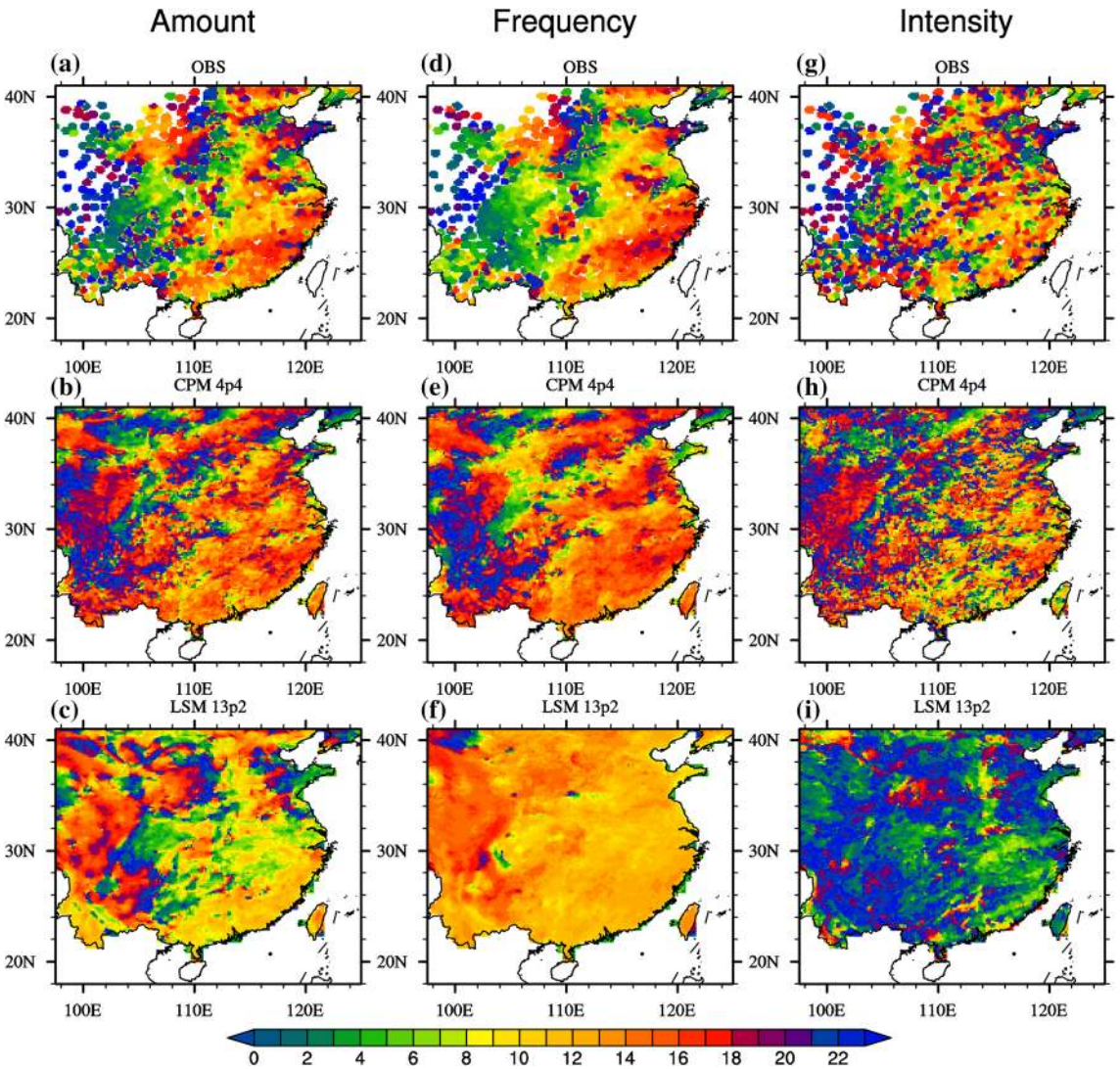

Fig. 3 Spatial distributions of the local solar time (colored; local solar time, hereafter "LST" in short) of the maximum (T_{max}) in the composite diurnal cycle of the summer mean precipitation characteristics. **a–c** Precipitation amount; **d–f** precipitation frequency; and **g–i** precipitation intensity from **a, d, g** 2420 rain gauge observations; **b, e, h** CPM 4p4 simulations; **c, f, i** LSM 13p2 simulations

peak over southern and northern China (Fig. 3b). The weaknesses of CPM 4p4 simulation lie in the spurious afternoon rainfall (around 1500 LST) over the eastern periphery of TP, and an hour earlier peaktime of the afternoon rainfall over southern China. Nonetheless, in comparison with LSM 13p2, the CPM 4p4 is superior at reproducing the diurnal cycle of precipitation F, including the later afternoon rainfall over southeastern China and the nocturnal rainfall over the eastern periphery of TP which is in a good agreement with the rain gauge observation (Fig. 3e).

We further divided eastern China into four sub-regions based on distinct diurnal features. The diurnal cycles of summer precipitation A, F and I from rain gauge data, CPM 4p4 and LSM 13p2 are shown in Fig. 4. Region 1 (the Upper Yangtze river-valley) is dominated by nocturnal rainfall (there is a large peak in rainfall around 0200 LST), which is clearly seen in the diurnal cycles of precipitation A, F and I (Fig. 4a, e, i). The CPM 4p4 performs reasonably well at reproducing the nocturnal rainfall over region 1, but it also has a spurious afternoon rainfall (around 1500 LST). Region 2 (Mei-yu region; Fig. 4b, f, j) and Region 3 (southern China; Fig. 4c, g, k) are dominated by the afternoon peak around 1600 LST in both precipitation A and F. The CPM 4p4 reproduces the afternoon rainfall peaks in Region 2 and Region 3, and also reproduces the secondary rainfall peaks in the early morning (around 0600 LST) over Region 3. By contrast, the LSM 13p2 has a 4-h earlier shift (until 1200 LST) in the timing of the afternoon rainfall peak. Region 4 (Fig. 4d, h, l) shows semi-diurnal rainfall peaks (with two peaks, of comparable magnitude: one in the early morning, the other in the afternoon). The peak around 0600 LST is mainly contributed by the precipitation F, the other peak after 1600 LST is primarily dominated by the precipitation I. The CPM 4p4 reproduces the afternoon

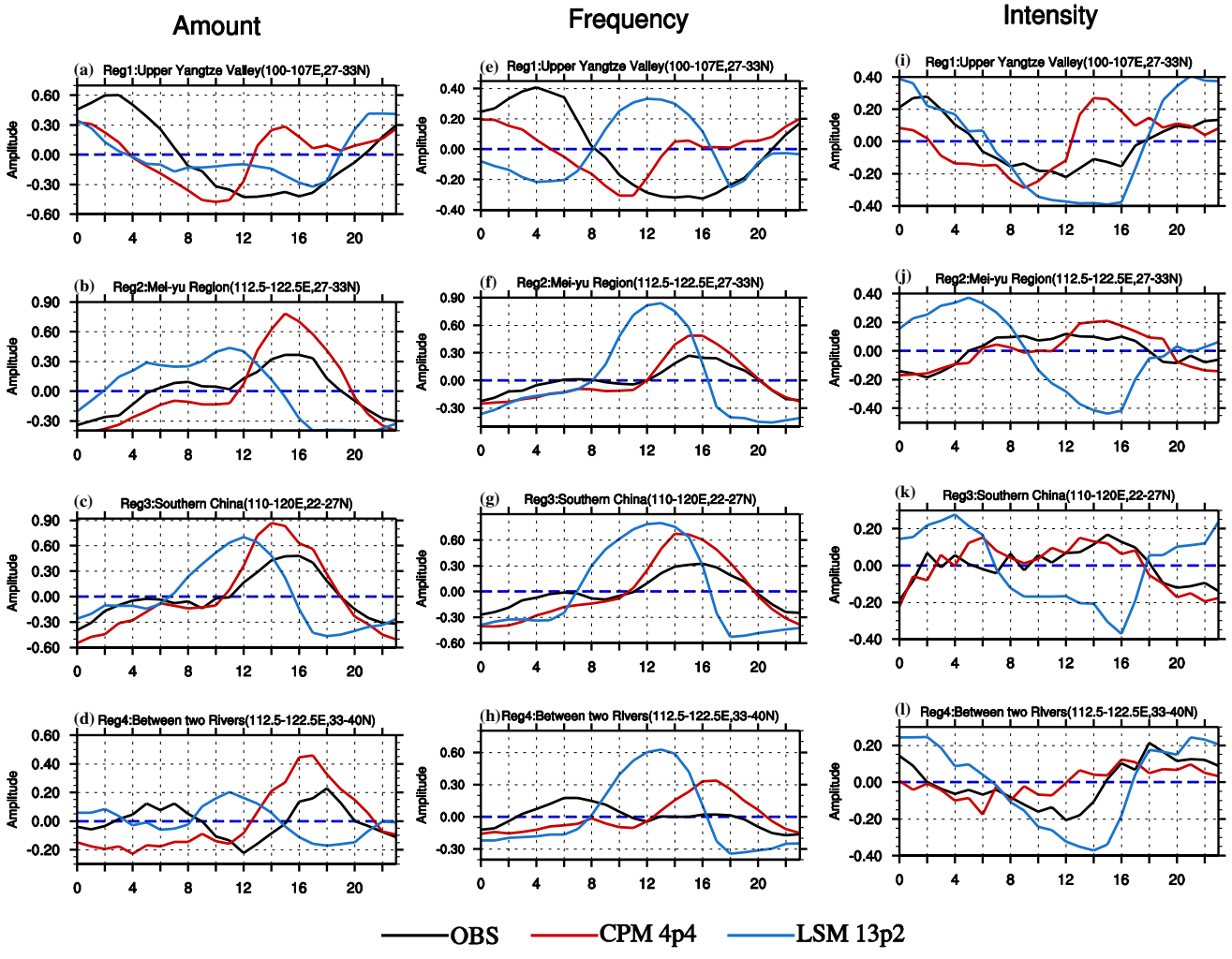

Fig. 4 Mean diurnal cycle of summer mean precipitation amount (first column), frequency (second column) and intensity (third column) (normalized according to Eq. 1) averaged over the four sub-regions (outlined in Fig. 1) from rain gauge data (OBS; black line), CPM 4p4 (red line) and LSM 13p2 (blue line). The unit of *x*-axis is LST in hours

peak but has an earlier shift of 2 h, along with an overestimation of the amplitude. The LSM 13p2 shows relatively low skill in reproducing the double diurnal peak over this region: it rains too frequently and too weakly, starts to rain too early in the afternoon, and has a rapid reduction in rainfall at sunset (around 1800 LST; Fig. 4d, h). Overall, CPM 4p4 performs better than LSM 13p2 in reproducing the characteristics of the diurnal cycle in all four sub-regions.

3.3 The diurnal cycle of large scale atmospheric circulations

The diurnal variation of wind fields over EASM, including the low-level wind, sea–land breeze, and surface wind, are fundamental circulation systems that modulate the diurnal cycle of rainfall (Yu et al. 2007b, 2009; Chen et al. 2009, 2010a, 2013, 2016). We examine the performance of models in reproducing the large scale circulation patterns by showing the diurnal evolution of the horizontal low-level (at 850 hPa) winds and equivalent potential temperature (EPT) in Fig. 5. Their vertical cross sections along the Yangtze River valley (27°N–33°N) among MERRA2 and model simulations are shown in Fig. 6. At 2000 BST (Fig. 5c, g, k), the winds are towards the TP and bring the warm and moist air mass to the upper Yangtze River valley. In addition, there exists an intense upward motion to the eastern periphery of the TP (Fig. 6c, g, k). This large-scale circulation is favorable for the nocturnal rainfall, until the intense upward motion becomes weaker and reverses to a descending motion at 0800 BST over the upper Yangtze River valley (Fig. 6a, e, i). The circulation pattern is consistent with the diurnal variation of rainfall (see the positive standardized rainfall from 2000 LST to 0800 LST; Fig. 4a). On the contrary, the Mei-yu region is dominated by a descending motion at 2000 BST (Fig. 6c, g, k). At 0200 BST, the low-level winds exhibit a clockwise rotation and become a southerly flow (Fig. 5d, h, l). In the morning (0800 BST), there exists a descending motion to the eastern periphery of the TP, and the low-level wind converges over the Mei-yu region (Fig. 5a, e, i). The LSM 13p2 produces a relatively stronger upward motion, with a value of -8.4×10^{-2} Pa s^{-1} at 500 hPa pressure level over the Mei-yu region (Fig. 6i), compared with the value of -6.2×10^{-2} Pa s^{-1} in MERRA2 (Fig. 6a) and -5.0×10^{-2} Pa s^{-1} in CPM 4p4 simulation (Fig. 6e). This is consistent with excessive rainfall over the Mei-yu region in LSM 13p2 in the morning (Fig. 6i).

In the afternoon (1400 BST), the low-level southwesterly weakens over southern China and the Mei-yu region, and the EPT of the air mass increases (Fig. 5b, f, j). In addition, the atmospheric conditions become unstable (higher EPT air near the surface and lower EPT air in the mid troposphere) and intense upward motions develop over the Mei-yu region (to the east of 115°E, Fig. 6b) which are consistent with the afternoon rainfall peak over the Mei-yu region (Figs. 4b, 6b). The upward motion over the Mei-yu region is relatively more intense in CPM 4p4 (Fig. 6f) compared with MERRA2 reanalysis (Fig. 6b).

We further checked the low level (at 850 hPa) wind speed and direction bias in both simulations (Fig. 7). There exists a systematic bias in both LSM 13p2 and CPM 4p4 simulations: the low-level southwesterly is stronger in both simulations. The wind biases in both models are more evident during the night-time and morning (at 0200 BST, Fig. 7d, h; at 0800 BST, Fig. 7a, e), when the low-level southwesterly flow intensifies. In the LSM 13p2 simulation, the wind speed is more than 4 m s^{-1} stronger than observed (Fig. 7h, e). The stronger winds bring moist-warm air from the South China Sea to the lower Yangtze River valley and, moreover, remain strong throughout the day. The excessive nocturnal wind speeds, are associated with enhanced upward motion over the Mei-yu region (Fig. 6), and may explain why the LSM 13p2 has excessive night-time and morning rainfall over the Mei-yu region. Compared with LSM 13p2 simulations, the CPM 4p4 performs better at reproducing the clockwise rotation of low-level large-scale circulation. The wind speed bias is reduced during night-time (at 0200 BST; Fig. 7d) and morning-time (at 0800 BST; Fig. 7a), and the meridional wind is more realistic over the Mei-yu region (Fig. 7a, d), this is consistent with the nocturnal rainfall being better simulated by CPM 4p4.

To further quantify the improvements in the diurnal cycle of low-level wind in CPM 4p4, Fig. 8 shows hodograph plots of low level (850 hPa) wind vectors over the Mei-yu region (Fig. 8a) and southern China (Fig. 8b). It is clear that the diurnal cycle of low level wind over both the Mei-yu region and southern China exhibits an inertial oscillation, the wind speed becomes larger during the night-time (from 2300 BST to 0200BST) and is minimal in the afternoon (between 1400 BST to 1700 BST). Both the LSM 13p2 and CPM 4p4 could simulate the wind direction and the inertial oscillation over the Mei-yu region and southern China, but LSM 13p2 overestimates the meridional wind over the Mei-yu region (Fig. 8a) and has a stronger wind speed over southern China (Fig. 8b). The CPM 4p4 performs better at reproducing the cycle of low level wind, in terms of both wind speed and wind direction over Mei-yu region and southern China. Based on previous studies (Du and Rotunno 2014; Du et al. 2014, 2015a, b; Shapiro et al. 2016), it is hypothesized that the improvement results from either a better representation of pressure gradient forcing or the turbulent mixing in CPM, but the details warrant further study.

3.4 Diurnal variation of rainfall along the Yangtze River valley

The Hovmöller diagrams of rainfall diurnal variation over the Yangtze River valley (averaged between 27°N and

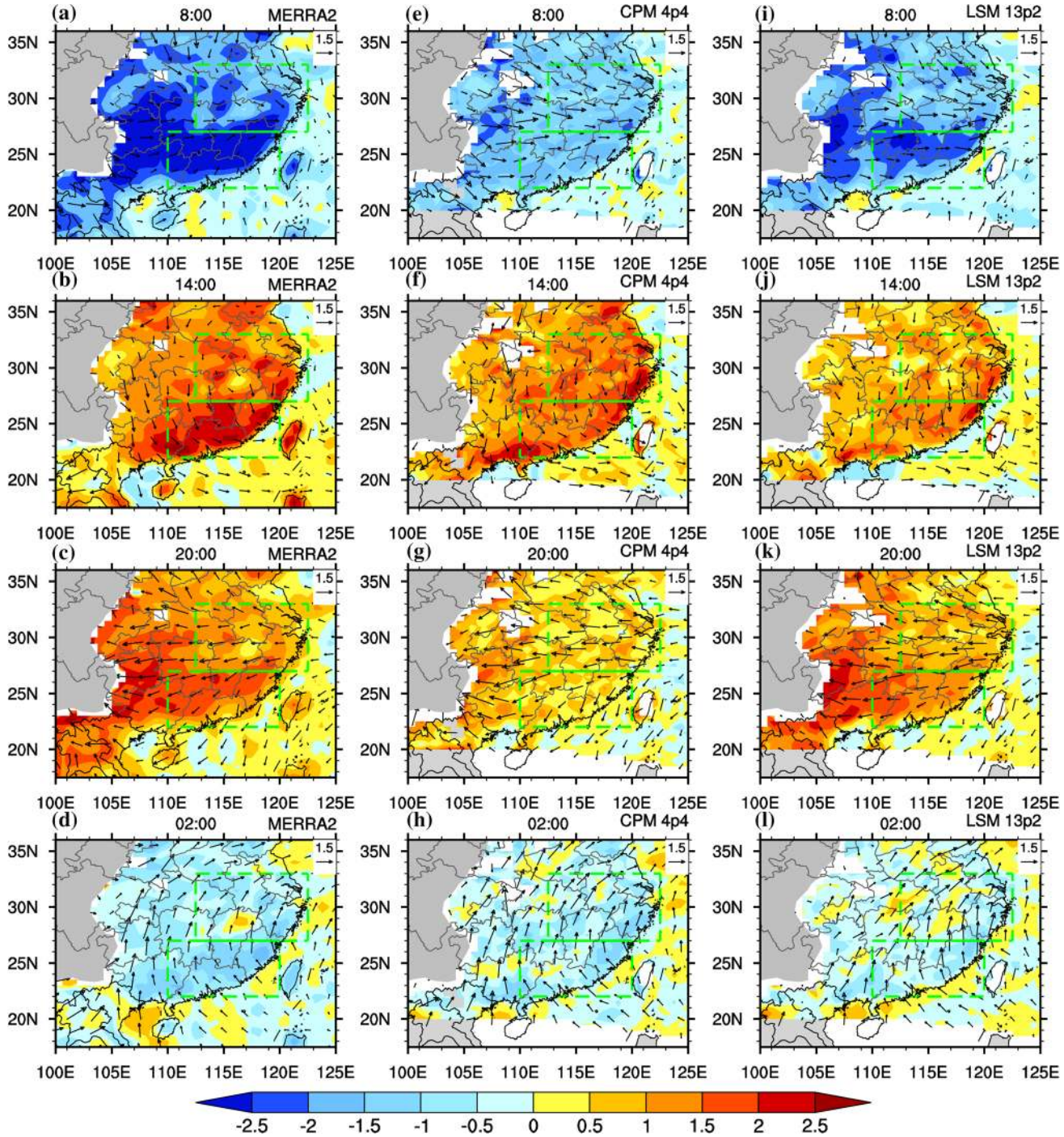

Fig. 5 JJA average for the wind vectors and equivalent potential temperature (EPT) anomalies (remove the daily mean values) at 850 hPa at 0800 Beijing Standard Time (BST), 1400 BST, 2000 BST, and 0200 BST in MERRA2 reanalyses (**a**–**d**), CPM 4p4 simulations (**e**–**h**) and LSM 13p2 simulations (**i**–**l**). Shading is the EPT (unit: K) and vectors indicate low level wind (unit: m s^{-1}) at 850 hPa. The two green rectangle boxes indicate the Mei-yu region (112.5°E–122.5°E, 27°N–33°N; upper box) and southern China (110°E–120°E, 22°N–27°N; bottom box). The areas higher than 1500 m are masked out

33°N) are shown in Fig. 9. There is an obvious eastward delay in the phase of the diurnal cycle along the Yangtze River valley (Fig. 9a). A prominent feature of summertime precipitation over the upper Yangtze River valley is that it occurs nocturnally. In addition, the rainfall maximum shows a 6-h delay (until around 0600 LST in the early morning) between the upper and middle Yangtze River valley (e.g., between 100°E and 108°E). This phase-shift comes from

the diurnal clockwise rotation of the low tropospheric circulation (Chen et al. 2010a). The "eastward-delayed diurnal phase transition" phenomenon is not evident to the east of 110°E where there is diurnally-synchronous rainfall over the lower reaches of the Yangtze River valley (i.e., the "Mei-yu" region), with the precipitation peaking around 1600 LST in the afternoon. The LSM 13p2 reproduces the nocturnal rainfall over the upper Yangtze River valley, but it has a spurious peak in the early afternoon (around 1400 LST; Fig. 9b). Due to the dependence on the convection scheme, rainfall often occurs in the morning to the east of 110°E in LSM 13p2 and thus shows an early-shifted phase compared with the rain gauge observation. For locally-forced convection, this sort of error is similar to those reported in previous studies and is typical of models with parametrized convection (Dai 2006; Guichard et al. 2010; Stephens et al. 2010). The CPM 4p4 successfully reproduces the nocturnal rainfall over the upper Yangtze River valley, but has a spurious afternoon rainfall (around 1500 LST; Fig. 9b). Relative to the LSM 13p2, the CPM 4p4 has a closer resemblance to the rain gauge observations, in terms of the phase of the diurnal cycle, over the areas to the east of 110°E that are dominated by the late afternoon rainfall. The weakness of CPM 4p4 is the overestimation of the magnitude of late afternoon rainfall over the Mei-yu region, and the afternoon precipitation in the middle of Yangtze River valley (around 105°E–110°E).

To understand the relationship between local atmospheric instability and afternoon rainfall peaks over the Mei-yu region, the vertical profile of MSE (calculated using Eq. 2) over Mei-yu region is investigated. The profiles of MSE anomalies (solid line; defined as the anomalies of the MSE profiles at each time, compared to the daily mean MSE profile for JJA in 2009) at every 0200 BST (blue) and 1400 BST (red) averaged for the Mei-yu region, and its temperature (c_pT; dashed lines) and moisture components (L_vq; dot-dashed lines) are shown in Fig. 10. In reanalysis (Fig. 10a, b), the afternoon rainfall over the Mei-yu region is associated with an anomalous higher MSE profile (red solid line in Fig. 10a, b), which has enhanced instability below 700 hPa, compared to the daily mean, and neutral above that level. The development of MSE gradients in the lower-troposphere in the afternoon is favorable for an upward motion and rainfall; in particular, compared to ERAIM and LSM 13p2, the MSE profile has larger positive perturbations in the lower troposphere in CPM 4p4, indicating the existence of more intense motions in the model.

In the afternoon, the c_pT term is largest near the surface and decreases with the altitude below 750 hPa in both reanalysis and models simulations, due to the daytime warming from the land surface. The diurnal variation of L_vq term is relatively smaller and negative near the surface (around 975 hPa) and becomes largest at lower troposphere (between 950 and 850 hPa). An anomalous profile of this shape is consistent with the occurrence of strengthened vertical transport of specific humidity by upward motions in the afternoon. Although there is also rainfall at night over the Mei-yu region, the MSE anomalies are stable and therefore are not favorable for the initiation of nocturnal convection (blue solid line in Fig. 10a, b). This suggests that the nocturnal rainfall over the Mei-yu region is likely to be contributed to by large-scale circulations, e.g., moisture convergence or down-stream advection of MCSs, and is less related to local surface-driven process than the afternoon rainfall.

Both the LSM 13p2 and CPM 4p4 simulations could reproduce the diurnal cycle of MSE profile (Fig. 10c, d). In the afternoon, LSM 13p2 and CPM 4p4 show enhanced vertical transport of humidity (red dot-dashed line in Fig. 10c, d). The L_vq term in CPM 4p4 (red dot-dashed line in Fig. 10d) is about twice large at its peak than that in LSM 13p2 (red dot-dashed line in Fig. 10c), suggesting that the vertical transport in CPM 4p4 is more vigorous which is consistent with the excessive rainfall in the model. In addition, the near surface value of the c_pT term in CPM 4p4 is also larger than LSM 13p2 (the red dashed line in Fig. 10d, c). Both of these two factors are consistent with the more unstable atmospheric conditions in CPM 4p4, which is favorable for upward motion and afternoon rainfall over the Mei-yu region.

To further explore the reason why the CPM 4p4 overestimate the late afternoon (1400 LST to 2000 LST) rainfall over the Mei-yu region, we compare the variation of upward motion in the afternoon (Fig. 11a–c) and surface sensible heat flux (Fig. 11d) derived from the MERRA2 reanalysis and model simulation. In the afternoon, the atmosphere near the surface in CPM 4p4 receives more surface sensible heat flux than those in LSM 13p2 and MERRA2 (Fig. 11d), leading to a more unstable atmosphere. At the same time, the upward motion in CPM 4p4 becomes intense (Fig. 11b) and is stronger than those in MERRA2 (Fig. 11a) and LSM 13p2 (Fig. 11c), which is consistent with the excessive precipitation in CPM 4p4. The more unstable atmosphere and enhanced upward motion in CPM 4p4 provide a favorable dynamical background for the overestimation of afternoon rainfall.

We further perform a moisture budget analysis to understand the water vapor supply for the afternoon rainfall (Fig. 11e). The evaporation rates are calculated from the latent heat fluxes derived from MERRA2 and model simulations. The late afternoon rainfall in CPM 4p4 (0.54 mm h^{-1}) is about twice as much as in the observations (0.30 mm h^{-1}; Fig. 11e). The convergence of water vapor into the Mei-yu region is 0.07 mm h^{-1} in the late afternoon, and the evaporation term is 0.22 mm h^{-1} in MERRA2 (Fig. 11e), demonstrating that the late afternoon rainfall over the Mei-yu region results from convective instabilities triggered by local heating. In CPM 4p4 from the contributions of local evaporation (0.18 mm h^{-1}) and large-scale convergence (0.23 mm h^{-1}) are comparable. The CPM 4p4 overestimates

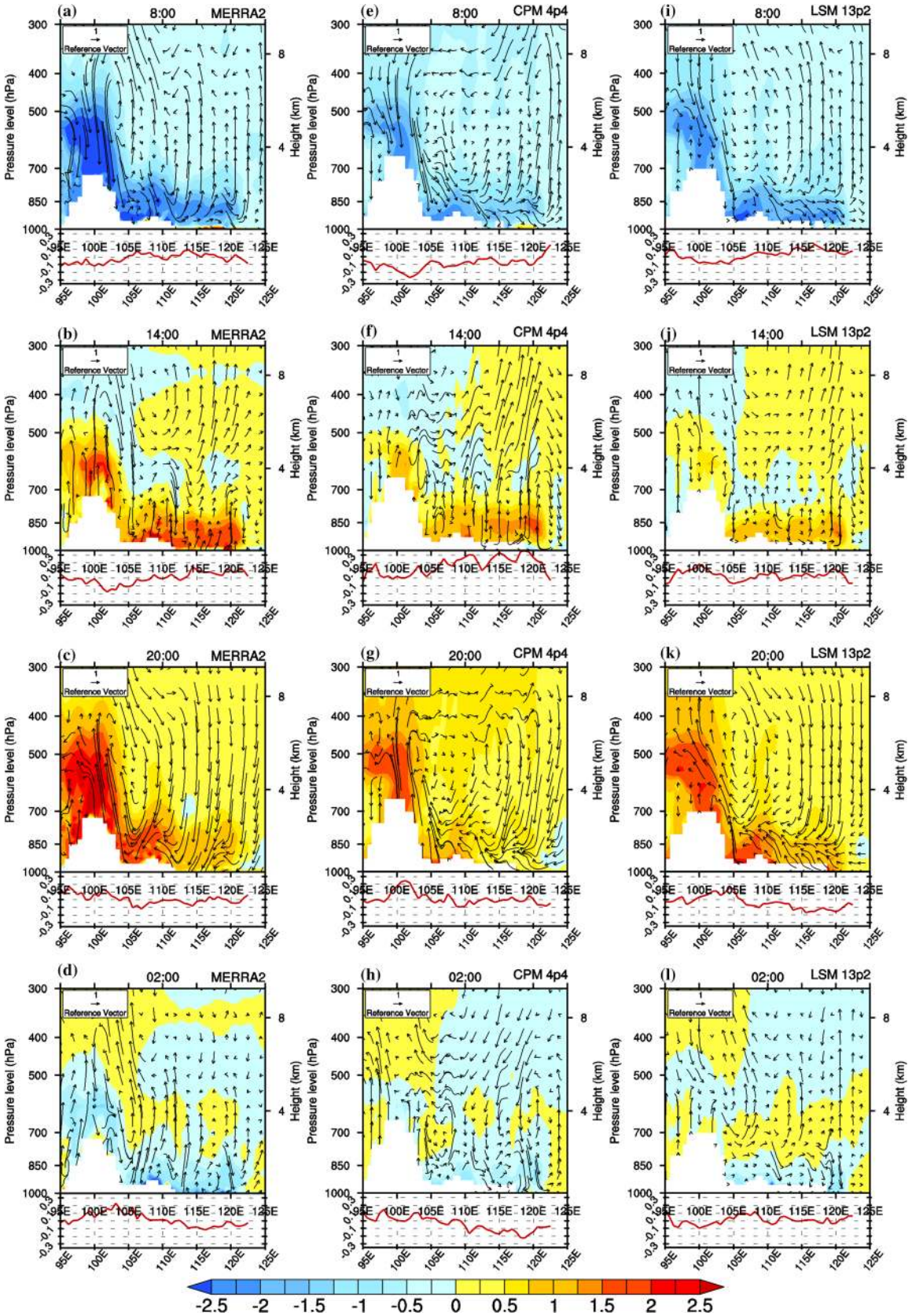
(a) 8:00 MERRA2
(e) 8:00 CPM 4p4
(i) 8:00 LSM 13p2
(b) 14:00 MERRA2
(f) 14:00 CPM 4p4
(j) 14:00 LSM 13p2
(c) 20:00 MERRA2
(g) 20:00 CPM 4p4
(k) 20:00 LSM 13p2
(d) 02:00 MERRA2
(h) 02:00 CPM 4p4
(l) 02:00 LSM 13p2
Reference Vector
Pressure level (hPa)
Height (km)
95E 100E 105E 110E 115E 120E 125E
-2.5 -2 -1.5 -1 -0.5 0 0.5 1 1.5 2 2.5

◂**Fig. 6** East–west cross sections of longitude-vertical circulation anomalies (remove the daily mean values; vectors: zonal wind, unit: m s^{-1}; omega, unit: -1.0×10^{-2} Pa s^{-1}), EPT (shading; unit: K) and the longitude profile of rainfall anomalies (3 h accumulated rainfall anomalies around each specific time; remove the daily mean values) based on the same region (red line of the lower part in each panel unit: mm h^{-1}), averaged between 27°N and 33°N at each time (0800 BST, 1400 BST, 2000 BST and 0200 BST) in the MERRA2 reanalysis and model simulations in the summer of 2009. **a**–**d** MERRA2 reanalysis; **e**–**h** CPM 4p4 simulations; **i**–**l** LSM 13p2 simulations

the convergence, compared to MERRA2 and LSM 13p2. Hence, one possible reason for the excessive rainfall in the CPM simulation, is that the convergence of the moisture flux is too large (0.23 mm h^{-1}) during the late afternoon compared with the MERRA2 reanalysis (0.07 mm h^{-1}) and LSM 13p2 (0.13 mm h^{-1}). This excess vapor water is then readily converted to rainfall because the model atmosphere has already been rendered too convectively unstable by a local surface-driven process (Fig. 11b, d).

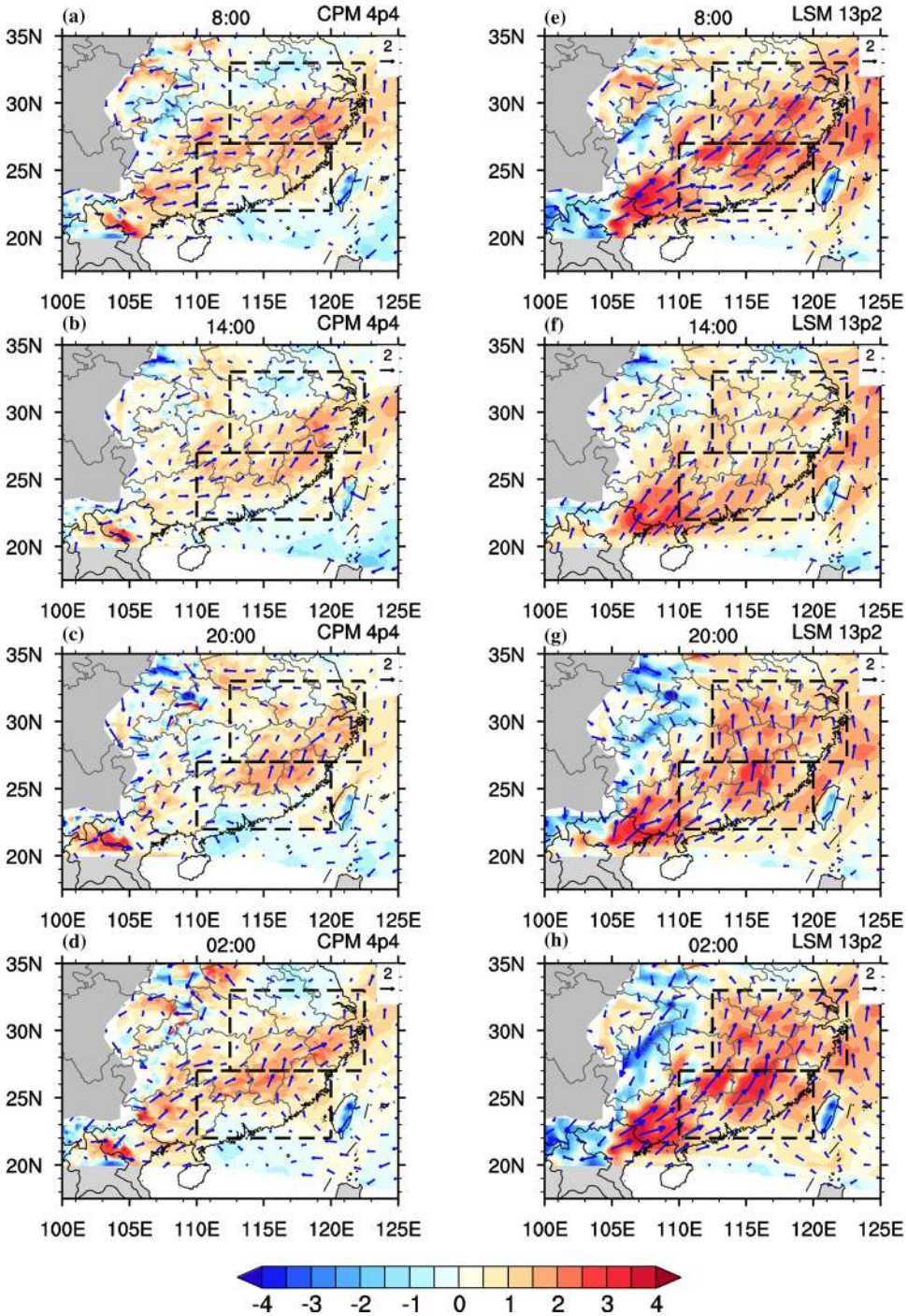

Fig. 7 Southwesterly wind bias (vectors, unit: m s^{-1}) and wind speed bias (shading, unit: m s^{-1}) at 850 hPa at **a** 0800, **b** 1400, **c** 2000, and **d** 0200 BST in CPM 4p4 simulations; **e**–**h** the same as **a**–**d**, but for LSM 13p2 simulations. The upper box indicates the Mei-yu region and the bottom box indicates southern China. The areas higher than 1500 m are masked out

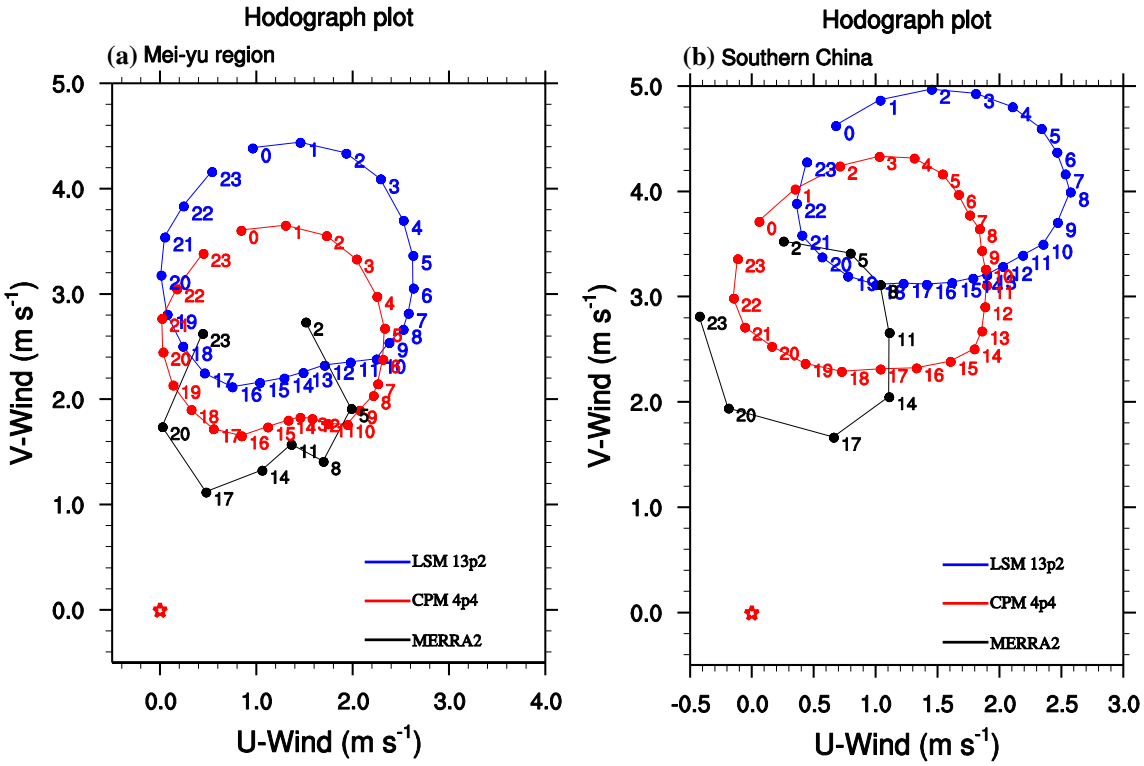

Fig. 8 The diurnal cycle of zonal and meridional wind fields (unit: m s^{-1}) at 850 hPa over Mei-yu region and southern China. The numbers in each plot indicate wind field at specific BST, the black line indicates the MERRA2 reanalysis, the red line indicates the CPM 4p4 simulations, and the blue line indicates the LSM 13p2 simulations, the pentagram indicates the origin

4 Summary and discussion

4.1 Summary

In this study, we have used rain gauge observations, reanalysis, and two high resolution regional model simulations (one convection-permitting, and one with parametrized convection), to evaluate, for the first time in the literature, the ability of a season long limited area CPM continuous simulation to reproduce the precipitation characteristics of the EASM, including the spatial distributions of summer mean precipitation A, F and I, as well as the diurnal cycle of precipitation. The performances of the models in the simulation of rainfall diurnal cycle are explained in the context of large-scale circulation variations. The main conclusions are summarized as follows:

1. The spatial distributions of summer mean precipitation A, F and I derived from CPM 4p4 show a relatively stronger resemblance to rain gauge observations, compared with LSM 13p2 simulations. The LSM 13p2 overestimate precipitation F but underestimate precipitation I over most parts of central eastern China. These biases are consistent with excessively frequent light-rainfall being produced by the model's convection scheme. By contrast, the CPM 4p4 could reasonably reproduce the precipitation F and I both in magnitude and spatial distribution, except for an overestimation of precipitation I and A over the EASM region.
2. The spatial distribution of diurnal rainfall cycle over eastern China indicates that there is an obvious regional dependence: nocturnal rainfall dominates the diurnal cycle over the eastern periphery of the TP; rainfall peaks in the afternoon over eastern and southern China. The CPM 4p4 model successfully reproduces the night-time rainfall over the eastern periphery of the TP but merges with a spurious afternoon rainfall peak in this region. The CPM 4p4 reasonably reproduces the afternoon peaks over southern China, whereas the LSM 13p2 produces most of its rainfall 3 h earlier (at around local time noon each day). Because the LSM 13p2 rains preferentially around local time noon, it is unable to replicate the observed spatial distributions of the diurnal-cycle phase. This is particularly obvious for the diurnal cycles of precipitation F, for which LSM 13p2 produces a spatial homogeneous distribution of phase with no clear evolution of phase between central and eastern China, and an intensity which has a nocturnal peak throughout

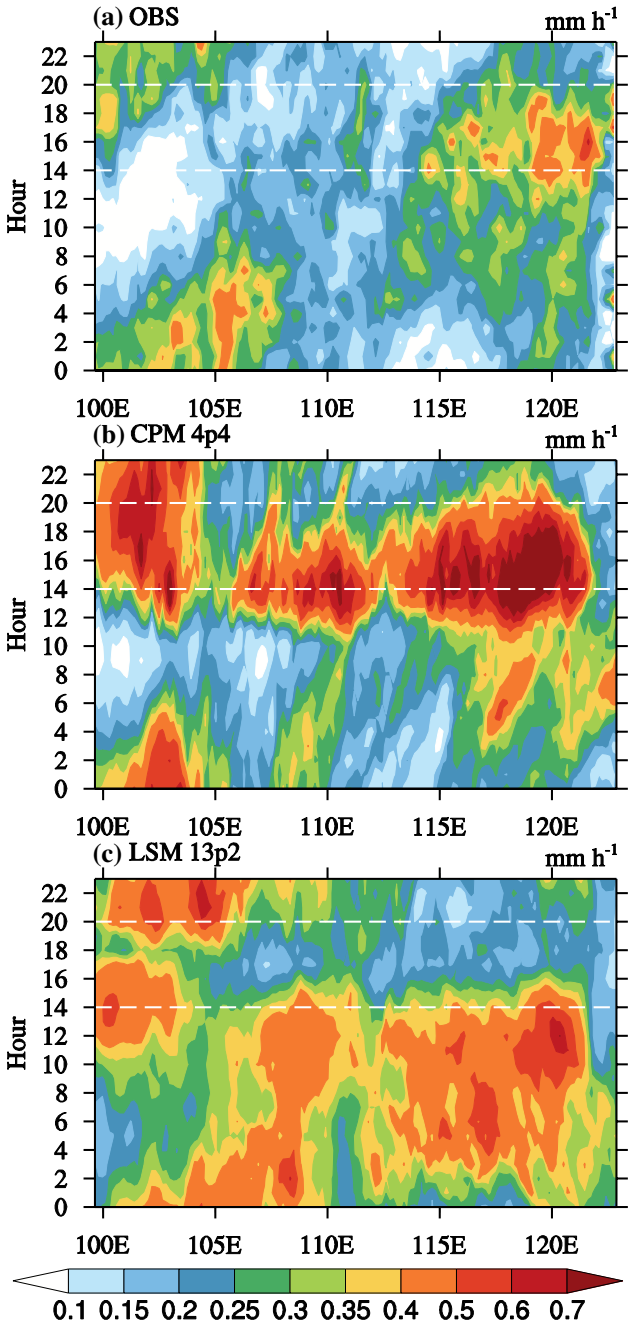

Fig. 9 Hovmöller diagram (LST versus 0.25 longitude bin) of hourly rainfall diurnal variations over Yangtze River region (averaged between 27°N and 33°N) for **a** rain gauge observations, **b** CPM 4p4 simulations and **c** LSM 13p2 simulations in the summer of 2009 (unit: mm h^{-1})

China in the LSM 13p2. The CPM 4p4 shows superiority in reproducing the diurnal cycle of precipitation F. What's more, the LSM 13p2 always produces morning rainfall to the east of 110°E, thus shows an early-shifted phase compared with the rain gauge observation. The CPM 4p4 could reasonably capture the late afternoon rainfall (around 1600 LST) over the Mei-yu region, but it overestimates the magnitude of precipitation.

3. The diurnal cycle of precipitation is highly correlated with the diurnal cycle of large scale circulation. Both the LSM 13p2 and CPM 4p4 simulations reproduced the diurnal clockwise rotation of the low level atmospheric circulations recorded by MERRA2, but the magnitude of the southwesterly wind was overestimated in both simulations. At 2000 BST, the winds are towards the TP, bringing the warm and moist air mass and there exists an intense upward motion over the upper Yangtze River valley in both MERRA2 and model simulations, the large-scale circulation is favorable for the nocturnal rainfall. After that the low-level wind exhibits a clockwise rotation and reaches its minimum over the Mei-yu region and southern China in the late afternoon (around 1700 BST). Over those two regions, there is a clear inertial oscillation of low level wind fields in MERRA2 reanalysis and both two simulations. In LSM 13p2, the southwesterly jet is too strong during the night time and early morning (from 2000 BST to 0800 BST). This is accompanied by overly rapid ascent over the Yangtze River valley, which leads to the spurious nocturnal and morning rainfall in these regions. Compared with LSM 13p2 simulations, the CPM 4p4 has a better performance in reproducing the low-level wind fields in both wind direction and wind speed over the Mei-yu region and southern China.
4. Excessive afternoon rainfall over the Mei-yu region in the CPM 4p4 simulation is related to the interactions between biases in local atmospheric stability and biases in large-scale moisture convergence. In the observations and the simulations, the local atmospheric state in the afternoon over the Mei-yu region is conducive to vertical motion and the production of convective rainfall. However, in CPM 4p4, the lower troposphere receives more sensible heat flux from the surface, and the MSE profile becomes more unstable for atmosphere below 850 hPa and whilst showing relatively little change in atmospheric stability above this level. Stronger intense upward motion is also found, which is consistent with the excessive late afternoon rainfall (0.54 mm h^{-1}) in CPM 4p4, compared with MERRA2 and LSM 13p2. In observation, the moisture budget analysis indicates that the late afternoon rainfall (0.30 mm h^{-1}) over the Mei-yu region is mainly contributed by the local evaporation (0.22 mm h^{-1}), compared with a minor contribution from large-scale convergence of water vapor transport (0.07 mm h^{-1}). The CPM 4p4 overestimate the convergence of water vapor transport (0.23 mm h^{-1}), and the atmosphere in CPM 4p4 converts the moisture from local evaporation and convergence of water vapor transport to precipitation readily, compared with MERRA2

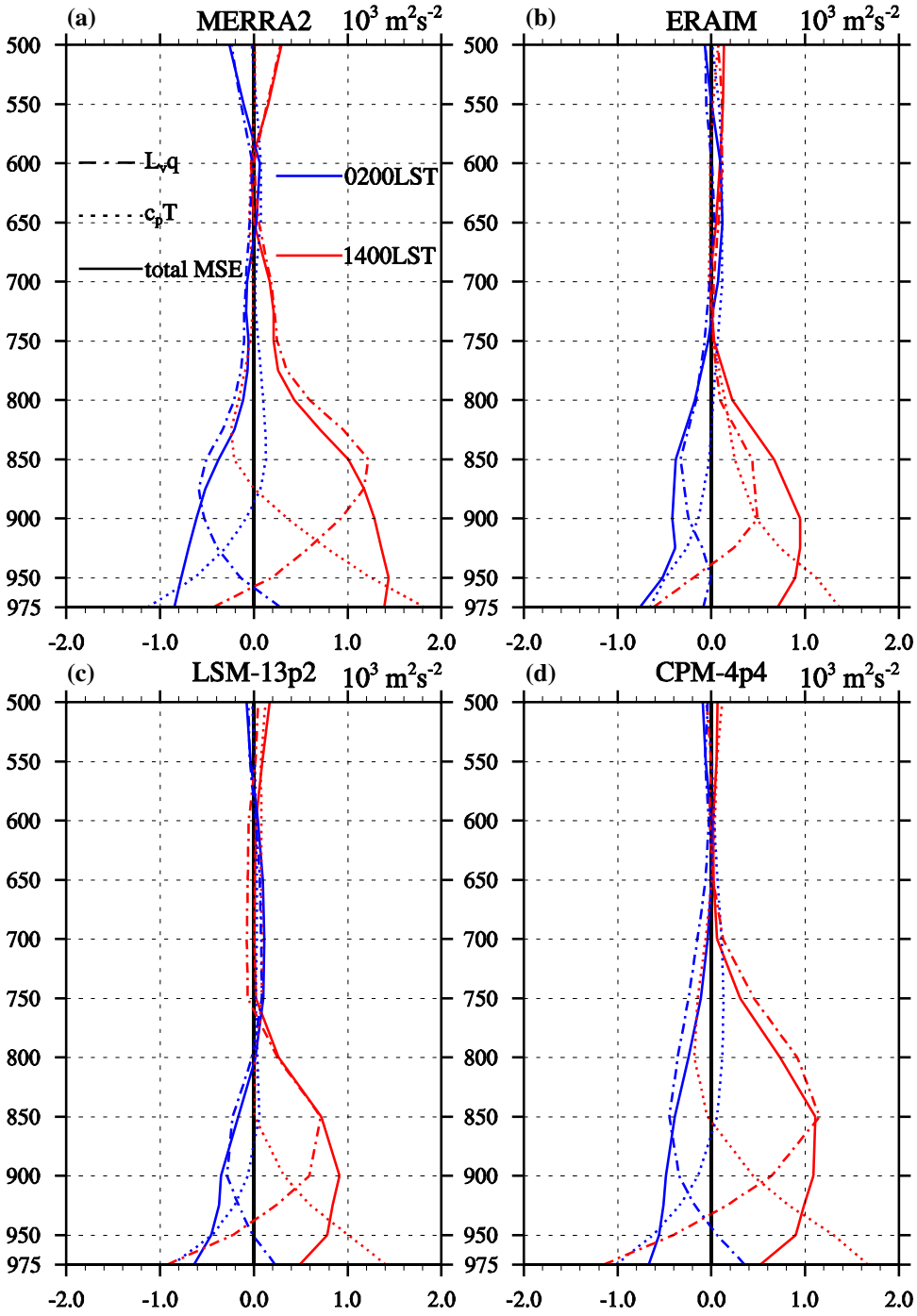

Fig. 10 **a** Profiles of MERRA2 total MSE (solid lines), temperature component (c_pT; dashed lines) and moisture components (L_vq; dot-dashed lines) anomalies (unit: 10^3 m^2 s^{-2}) averaged over the Mei-yu region at 1400 LST (red) and 0200 LST (blue); **b** the same as **a**, but for ERAIM reanalysis; **c, d** as in **a**, but for the **c** LSM 13p2 simulations and **d** CPM 4p4 simulations

and LSM 13p2. Both the enhanced unstable atmosphere and more convergence of water vapor help explain the excessive late afternoon rainfall over the Mei-yu region in the CPM 4p4 simulation.

4.2 Discussion

Since the added value of CPMs is often found at fine temporal and spatial scales, as well as the extreme events, such as mesoscale convective systems (Feng et al. 2016; Prein et al. 2017a, c), heavy downpours (Li et al. 2012; Mahoney et al. 2012; Ban et al. 2014; Zhu et al. 2018) and hourly precipitation extremes (Kendon et al. 2014; Ban et al. 2014, 2015; Chen et al. 2016; Prein et al. 2017b), more high quality observational datasets over EASM at high temporal and spatial resolution (including precipitation, surface temperature and other atmospheric variables) are needed, to make a robust evaluation on the performances of CPMs.

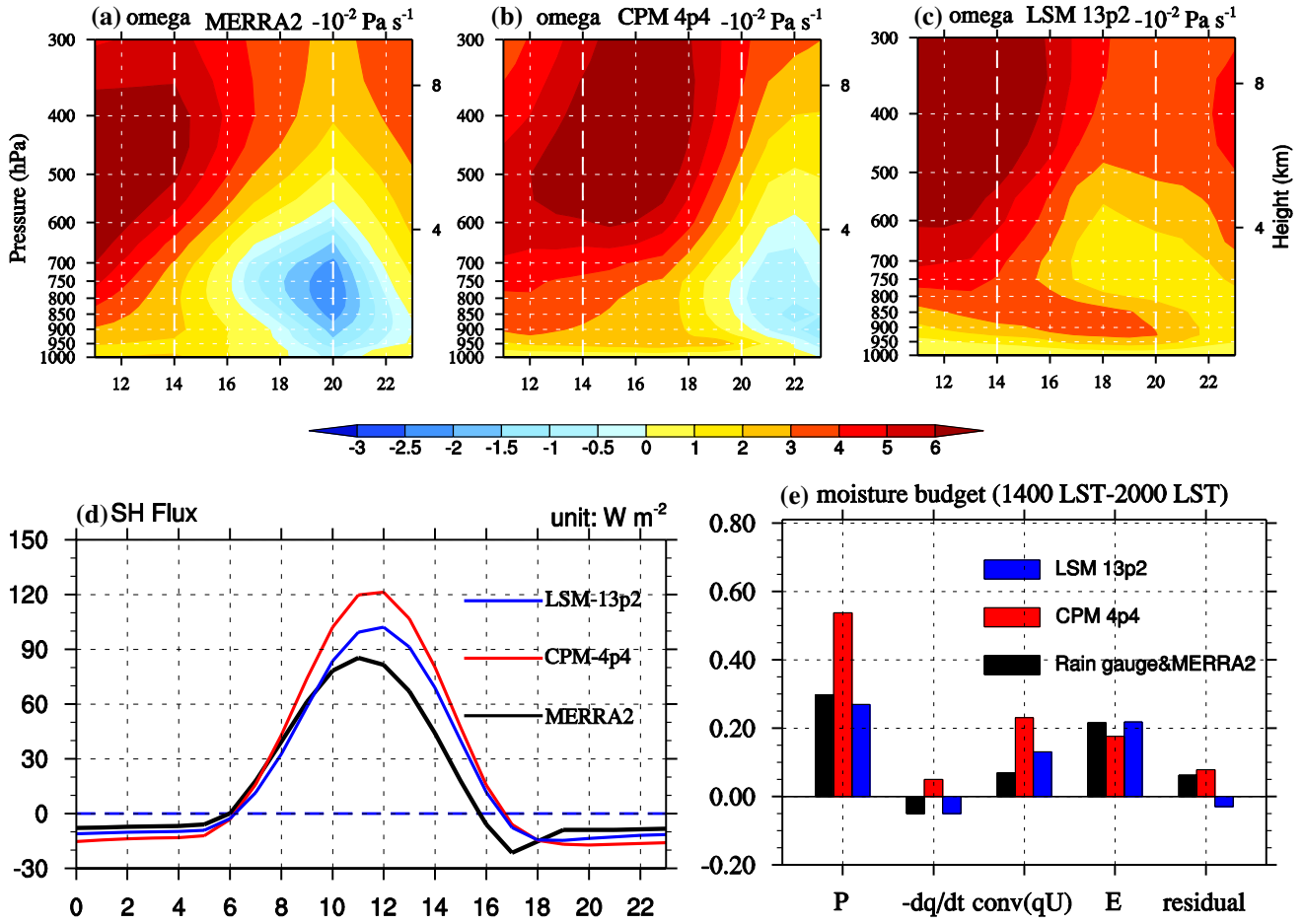

Fig. 11 Diurnal variations of upward motion (unit: -1.0×10^{-2} Pa s^{-1}) from 1100 LST to 2300 LST over Mei-yu region, from **a** MERRA2 reanalysis, **b** CPM 4p4 simulation and **c** LSM 13p2 simulation; **d** diurnal variations of surface sensible heat flux among MERRA2 reanalysis and model simulations over Mei-yu region (unit: W m^{-2}); **e** Moisture budget components among observation and model simulations from 1400 LST to 2000 LST over Mei-yu region (unit: mm h^{-1}), here P and E indicate precipitation and evaporation, respectively. "$-$dq/dt" denotes the changes of local moisture storage, the "conv(qU)" denotes convergence of integrated moisture flux, "residual" indicates the residual term

In addition, the diurnal cycle of large-scale circulations is known to modulate the diurnal cycle of precipitation over East Asia. For instance, during the warm-season there is a close relationship between the southwesterly low level jet (LLJ) and heavy rainfall over northern Taiwan (Chen et al. 2005) and in the middle and lower reaches of Yangtze River valley (Luo and Chen 2015; Chen et al. 2017) that has been reported for synoptic scale aspect. Recent studies (Du et al. 2014, 2015a, b) have elucidated the diurnal cycle of LLJ in terms of the classical theories of Blackadar (1957) and Holton (1967). It has been shown that the LLJ undergoes forced-damped quasi-diurnal oscillations due to the diurnal variations of turbulent mixing in the boundary layer and large-scale gradients in geopotential height. For example, turbulent frictional effects are largest in the afternoon (due to surface-driven vertical mixing), and smallest in the early morning. The ability of a model to represent these variations may play a significant role in simulating the diurnal cycle and mean-state of the LLJ. In this study, we show evidences that the CPM 4p4 has some added values in simulating the low-level wind over southern China and Mei-yu region, further studies are needed to understand the added values in CPM, in particular the relationship between the diurnal cycle of convection and large-scale circulations.

Long-duration CPM simulations could be useful for understanding the climatological effects of propagating mesoscale convective system (MCS) triggered in the lee of mountains. Globally, MCS is a major cause of extreme precipitation and is a common feature downstream of high topography such as the Rockies and the TP (Carbone et al. 2002; Wang et al. 2004, 2012; Chen et al. 2013; Feng et al. 2016). However, most state-of-the-art climate models can not adequately simulate the organized MCS (Bukovsky and Karoly 2011; Kooperman et al. 2014), in comparison to

CPM (Prein et al. 2017a, c). The TP is the highest and largest plateau in the world, previous studies have shown that eastward-propagating MCSs over EASM strongly influence the downstream rainfall and its diurnal cycle (Chen et al. 2013, 2014; Luo et al. 2014; Luo and Chen 2015), but there are only limited efforts devoted to the CPM simulation of synoptic scale. CPM modeling of MCSs over the TP and their eastward propagation deserves further study.

Acknowledgements This work was jointly supported by the National Natural Science Foundation of China under Grant Nos. 41420104006, 41330423, 41405103 and International Partnership Program of Chinese Academy of Sciences under Grant Nos. 134111KYSB20160031. Haoming Chen and Jian Li were supported by the National Natural Science Foundation of China under Grant Nos. 91637210, 41375004. Chan Xiao was supported by the National Key R&D Program of China (Grant No. 2016YFE0102400). Kalli Furtado was supported by the UK-China Research & Innovation Partnership Fund through the Met Office Climate Science for Service Partnership (CSSP) China as part of the Newton Fund. The authors wish to thank the National Meteorological Information Center of China Meteorological Administration for providing the station data, the Global Modeling and Assimilation Office for providing the MERRA2 reanalysis data and the European Centre for Medium-Range Weather Forecasts for the ERAIM reanalysis data.

References

Asai T, Ke S, Kodama Y (1998) Diurnal variability of cloudiness over East Asia and the western Pacific Ocean as revealed by GMS during the warm season. J Meteorol Soc Jpn Ser II 76(5):675–684

Ban N, Schmidli J, Schär C (2014) Evaluation of the convection-resolving regional climate modeling approach in decade-long simulations. J Geophys Res 119(13):7889–7907. https://doi.org/10.1002/2014JD021478

Ban N, Schmidli J, Schär C (2015) Heavy precipitation in a changing climate: does short-term summer precipitation increase faster? Geophys Res Lett 42(4):1165–1172. https://doi.org/10.1002/2014GL062588

Benedict J, Randall D (2009) Structure of the Madden–Julian oscillation in the superparameterized CAM. J Atmos Sci 66(11):3277–3296. https://doi.org/10.1175/2009JAS3030.1

Birch C, Parker D, Marsham J et al (2014) A seamless assessment of the role of convection in the water cycle of the West African Monsoon. J Geophys Res 119:2890–2912. https://doi.org/10.1002/2013JD020887

Birch C, Webster S, Peatman S et al (2016) Scale interactions between the MJO and the Western Maritime Continent. J Clim 29:2471–2492. https://doi.org/10.1175/JCLI-D-15-0557.1

Blackadar AK (1957) Boundary layer wind maxima and their significance for the growth of nocturnal inversions. Bull Am Meteorol Soc 38:283–290

Brockhaus P, Lüthi D, Schär C (2008) Aspects of the diurnal cycle in a regional climate model. Meteorol Z 17:433–443. https://doi.org/10.1127/0941-2948/2008/0316

Brown A, Milton S, Cullen M et al (2012) Unified modeling and prediction of weather and climate: a 25-year journey. Bull Am Meteorol Soc 93(12):1865–1877. https://doi.org/10.1175/BAMS-D-12-00018.1

Bukovsky MS, Karoly DJ (2009) Precipitation simulations using WRF as a nested regional climate model. J Appl Meteorol Clim 48:2152–2159. https://doi.org/10.1175/2009JAMC2186.1

Bukovsky MS, Karoly DJ (2011) A regional modeling study of climate change impacts on warm-season precipitation in the central United States. J Clim 24(7):1985–2002. https://doi.org/10.1175/2010JCLI3447.1

Carbone RE, Tuttle JD, Ahijevych DA, Trier SB (2002) Inferences of predictability associated with warm season precipitation episodes. J Atmos Sci 59(13):2033–2056

Chen D, Dai A (2018) Dependence of estimated precipitation frequency and intensity on data resolution. Clim Dyn 50(9–10):3625–3647. https://doi.org/10.1007/s00382-017-3830-7

Chen GTJ, Wang CC, Lin DTW (2005) Characteristics of low-level jets over northern Taiwan in Meiyu season and their relationship to heavy rain events. Mon Weather Rev 133(1):20–43

Chen G, Sha W, Iwasaki T (2009) Diurnal variation of precipitation over southeastern China: 2. Impact of the diurnal monsoon variability. J Geophys Res 114:D21105. https://doi.org/10.1029/2009JD012181

Chen H, Yu R, Li J, Yuan W, Zhou T (2010a) Why nocturnal long-duration rainfall presents an eastward-delayed diurnal phase of rainfall down the Yangtze River Valley. J Clim 23(4):905–917. https://doi.org/10.1175/2009JCLI3187.1

Chen H, Zhou T, Neale R, Wu X, Zhang G (2010b) Performance of the new NCAR CAM3.5 in East Asian summer monsoon simulations: sensitivity to modifications of the convection scheme. J Clim 23(13):3657–3675. https://doi.org/10.1175/2010JCLI3022.1

Chen G, Sha W, Sawada M, Iwasaki T (2013) Influence of summer monsoon diurnal cycle on moisture transport and precipitation over eastern China. J Geophys Res 118(8):3163–3177. https://doi.org/10.1002/jgrd.50337

Chen G, Yoshida R, Sha W, Iwasaki T (2014) Convective instability associated with the eastward-propagating rainfall episodes over eastern China during the warm season. J Clim 27(6):2331–2339. https://doi.org/10.1175/JCLI-D-13-00443.1

Chen X, Zhang F, Zhao K (2016) Diurnal variations of the land–sea breeze and its related precipitation over South China. J Atmos Sci 73(12):4793–4815. https://doi.org/10.1175/JAS-D-16-0106.1

Chen G, Sha W, Iwasaki T, Wen Z (2017) Diurnal cycle of a heavy rainfall corridor over East Asia. Mon Weather Rev 145(8):3365–3389

Chou C, Lan CW (2012) Changes in the annual range of precipitation under global warming. J Clim 25(1):222–235. https://doi.org/10.1175/JCLI-D-11-00097.1

Covey C, Gleckler PJ, Doutriaux C, Williams DN, Dai A, Fasullo J, Trenberth KE, Berg A (2016) Metrics for the diurnal cycle of precipitation: toward routine benchmarks for climate models. J Clim 29(12):4461–4471. https://doi.org/10.1175/JCLI-D-15-0664.1

Cressman GP (1959) An operational objective analysis system. Mon Weather Rev 87(10):367–374. https://doi.org/10.1175/1520-0493(1959)087<0367:AOOAS>2.0.CO;2

Cullen MJP (1993) The unified forecast climate model. Aust Meteorol Mag 122(1449):81–94

Dai A (2001) Global precipitation and thunderstorm frequencies. Part II: diurnal variations. J Clim 14(6): 1112–1128. https://doi.org/10.1175/1520-0442(2001)014<1112:GPATFP>2.0.CO;2

Dai A (2006) Precipitation characteristics in eighteen coupled climate models. J Clim 19(18):4605–4630. https://doi.org/10.1175/JCLI3884.1

Dai A, Deser C (1999) Diurnal and semidiurnal variations in global surface wind and divergence fields. J Geophys Res 104(D24):31109–31125

Dai A, Trenberth KE (2004) The diurnal cycle and its depiction in the Community Climate System Model. J Clim 17(5):930–951. https://doi.org/10.1175/1520-0442(2004)017<0930:TDCAID>2.0.CO;2

Dai A, Giorgi F, Trenberth KE (1999) Observed and model simulated diurnal cycles of precipitation over the contiguous US. J Geophys Res 104(D6):6377–6402. https://doi.org/10.1029/98JD02720

Dai A, Lin X, Hsu KL (2007) The frequency, intensity, and diurnal cycle of precipitation in surface and satellite observations over low- and mid-latitudes. Clim Dyn 29(7–8):727–744. https://doi.org/10.1007/s00382-007-0260-y

Dai A, Rasmussen R, Liu C, Ikeda K, Prein AF (2017) A new mechanism for warm-season precipitation response to global warming based on convection-permitting simulations. Clim Dyn. https://doi.org/10.1007/s00382-017-3787-6

Davies T, Cullen MJP, Malcolm AJ, Mawson MH, Staniforth A, White AA, Wood N (2005) A new dynamical core for the Met Office's global and regional modelling of the atmosphere. Q J R Meteorol Soc 131(608):1759–1782. https://doi.org/10.1256/qj.04.101

Dee DP et al (2011) The ERA-interim reanalysis: configuration and performance of the data assimilation system. Q J R Meteorol Soc 137(656):553–597. https://doi.org/10.1002/qj.828

Donlon CJ, Martin M, Stark JD, Roberts-Jones J, Fiedler E, Wimmer W (2012) The operational sea surface temperature and sea ice analysis (OSTIA). Remote Sens Environ 116:140–158. https://doi.org/10.1016/j.rse.2010.10.0172011

Du Y, Rotunno R (2014) A simple analytical model of the nocturnal low-level jet over the Great Plains of the United States. J Atmos Sci 71(10):3674–3683. https://doi.org/10.1175/JAS-D-14-0060.1

Du Y, Zhang Q, Chen YL, Zhao Y, Wang X (2014) Numerical simulations of spatial distributions and diurnal variations of low-level jets in China during early summer. J Clim 27(15):5747–5767. https://doi.org/10.1175/JCLI-D-13-00571.1

Du Y, Chen YL, Zhang Q (2015a) Numerical simulations of the boundary layer jet off the southeastern coast of China. Mon Weather Rev 143(4):1212–1231. https://doi.org/10.1175/mwr-d-14-00348.1

Du Y, Rotunno R, Zhang Q (2015b) Analysis of WRF-simulated diurnal boundary layer winds in eastern China using a simple 1D model. J Atmos Sci 72(2):714–727. https://doi.org/10.1175/JAS-D-14-0186.1

Ebita A et al (2011) The Japanese 55-year reanalysis "JRA-55": an interim report. SOLA 7:149–152. https://doi.org/10.2151/sola.2011-038

Feng Z, Leung LR, Hagos S, Houze RA, Burleyson CD, Balaguru K (2016) More frequent intense and long-lived storms dominate the springtime trend in central US rainfall. Nat Commun 7:13429. https://doi.org/10.1038/ncomms13429

Flato G, Marotzke J, Abiodun B, Braconnot P, Chou SC, Collins W, Cox P, Driouech F, Emori S, Eyring V, Forest C, Gleckler P, Guilyardi E, Jakob C, Kattsov V, Reason C, Rummukainen M (2013) Evaluation of climate models. In: Stocker TF, Qin D, Plattner GK, Tignor M, Allen SK, Boschung J, Nauels A, Xia Y, Bex V, Midgley PM (eds) Climate change 2013: the physical science basis. Cambridge University Press, Cambridge, New York, 741–866

Fosser G, Khodayar S, Berg P (2015) Benefit of convection permitting climate model simulations in the representation of convective precipitation. Clim Dyn 44(1–2):45–60. https://doi.org/10.1007/s00382-014-2242-1

Fosser G, Khodayar S, Berg P (2017) Climate change in the next 30 years: what can a convection-permitting model tell us that we did not already know? Clim Dyn 48(5–6):1987–2003. https://doi.org/10.1007/s00382-016-3186-4

Gelaro R, Mccarty W, Suárez MJ et al (2017) The modern-era retrospective analysis for research and applications, version 2 (MERRA-2). J Clim 30(14):5419–5454. https://doi.org/10.1175/JCLI-D-16-0758.1

Grant ALM (2001) Cloud-base fluxes in the cumulus-capped boundary layer. Q J R Meteorol Soc 127(572):407–421

Gregory D, Rowntree PR (1990) A mass flux convection scheme with representation of cloud ensemble characteristics and stability-dependent closure. Mon Weather Rev 118(7): 1483–1506. https://doi.org/10.1175/1520-0493(1990)118<1483:AMFCSW>2.0.CO;2

Guichard F, Petch JC, Redelsperger JL et al (2004) Modelling the diurnal cycle of deep precipitating convection over land with cloud-resolving models and single column models. Q J R Meteorol Soc 130(604):3139–3172. https://doi.org/10.1256/qj.03.145

Guichard F, Asencio N, Peugeot C et al (2010) An intercomparison of simulated rainfall and evapotranspiration associated with a mesoscale convective system over West Africa. Weather Forecast 25(1):37–60. https://doi.org/10.1175/2009WAF2222250.1

Hohenegger C, Brockhaus P, Bretherton CS, Schär C (2009) The soil moisture-precipitation feedback in simulations with explicit and parameterized convection. J Clim 22(19):5003–5020. https://doi.org/10.1175/2009JCLI2604.1

Holloway CE, Woolnough SJ, Lister GMS (2012) Precipitation distributions for explicit versus parameterised convection in a large-domain high-resolution tropical case study. Q J R Meteorol Soc 138(668):1692–1708. https://doi.org/10.1002/qj.1903

Holton JR (1967) The diurnal boundary layer wind oscillation above sloping terrain. Tellus 19(2):199–205. https://doi.org/10.3402/tellusa.v19i2.9766

Jiang Z, Zhang DL, Xia R et al (2017) Diurnal variations of presummer rainfall over southern China. J Clim 30(2):755–773. https://doi.org/10.1175/JCLI-D-15-0666.1

Kendon EJ, Roberts NM, Fowler HJ et al (2014) Heavier summer downpours with climate change revealed by weather forecast resolution model. Nat Clim Change 4(7):570–576. https://doi.org/10.1038/nclimate2258

Klocke D, Brueck M, Hohenegger C, Stevens B (2017) Rediscovery of the doldrums in storm-resolving simulations over the tropical Atlantic. Nat Geosci 10(12):891. https://doi.org/10.1038/s41561-017-0005-4

Kooperman GJ, Pritchard MS, Somerville RCJ (2013) Robustness and sensitivities of central US summer convection in the super-parameterized CAM: multi-model intercomparison with a new regional EOF index. Geophys Res Lett 40(12):3287–3291. https://doi.org/10.1002/grl.50597

Kooperman GJ, Pritchard MS, Somerville RCJ (2014) The response of US summer rainfall to quadrupled CO2 climate change in conventional and superparameterized versions of the NCAR community atmosphere model. J Adv Model Earth Syst 6(3):859–882. https://doi.org/10.1002/2014MS000306

Lau WKM, Kim KM (2017) Competing influences of greenhouse warming and aerosols on Asian summer monsoon circulation and rainfall. Asia-Pacific J Atmos Sci 53(2):181–194. https://doi.org/10.1007/s13143-017-0033-4

Lean HW, Clark PA, Dixon M, Roberts NM, Fitch A, Forbes R, Halliwell C (2008) Characteristics of high-resolution versions of the Met Office Unified Model for forecasting convection over the United Kingdom. Mon Weather Rev 136(9):3408–3424. https://doi.org/10.1175/2008MWR2332.1

Li J (2017) Hourly station-based precipitation characteristics over the Tibetan Plateau. Int J Climatol. https://doi.org/10.1002/joc.5281

Li F, Rosa D, Collins WD, Wehner MF (2012) "Super-parameterization": a better way to simulate regional extreme precipitation? J Adv Model Earth Syst 4(2):M04002. https://doi.org/10.1029/2011MS000106

Li P, Zhou T, Chen X (2017) Water vapor transport for spring persistent rains over southeastern China based on five reanalysis datasets. Clim Dyn 6:1–15. https://doi.org/10.1007/s00382-017-3680-3

Liang XZ, Li L, Dai A, Kunkel KE (2004) Regional climate model simulation of summer precipitation diurnal cycle over the United States. Geophys Res Lett 31(24):L24208. https://doi.org/10.1029/2004GL021054

Lin R, Zhou T, Qian Y (2014) Evaluation of global monsoon precipitation changes based on five reanalysis datasets. J Clim 27(3):1271–1289. https://doi.org/10.1175/JCLI-D-13-00215.1

Liu C, Ikeda K, Rasmussen RM, Barlage M, Newman AJ, Prein AF, Chen F, Chen L, Clark M, Dai A, Dudhia J, Eidhammer T, Gochis D, Gutmann E, Kurkute S, Li Y, Thompson G, Yates D (2017) Continental-scale convection-permitting modeling of the current and future climate of North America. Clim Dyn 49(1–2):71–95. https://doi.org/10.1007/s00382-016-3327-9

Luo Y, Chen Y (2015) Investigation of the predictability and physical mechanisms of an extreme-rainfall-producing mesoscale convective system along the Meiyu front in East China: an ensemble approach. J Geophys Res 120(20):10593–10618. https://doi.org/10.1002/2015JD023584

Luo Y, Gong Y, Zhang DL (2014) Initiation and organizational modes of an extreme-rain-producing mesoscale convective system along a Mei-Yu Front in East China. Mon Weather Rev 142(1):203–221

Ma S, Zhou T (2015) Precipitation changes in wet and dry seasons over the 20th century simulated by two versions of the FGOALS model. Adv Atmos Sci 32(6):839–854. https://doi.org/10.1007/s00376-014-4136-x

Mahoney K, Alexander MA, Thompson G, Barsugli JJ, Scott JD (2012) Changes in hail and flood risk in high-resolution simulations over Colorado's mountains. Nat Clim Change 2(2):125–131. https://doi.org/10.1038/NCLIMATE1344

Marsham JH, Dixon N, Garcia-Carreras L, Lister GMS, Parker DJ, Knippertz P, Birch C (2013) The role of moist convection in the West African monsoon system: insights from continental-scale convection-permitting simulations. Geophys Res Lett 40(9):1843–1849. https://doi.org/10.1002/grl.50347

Miura H, Satoh M, Nasuno T, Noda AT, Oouchi K (2007) A Madden–Julian oscillation event realistically simulated by a global cloud-resolving model. Science 318(5857):1763–1765. https://doi.org/10.1126/science

Neupane N, Cook KH (2013) A nonlinear response of Sahel rainfall to Atlantic warming. J Clim 26(18):7080–7096. https://doi.org/10.1175/JCLI-D-12-00475.1

Pearson KJ, Hogan RJ, Allan RP, Lister GMS, Holloway CE (2010) Evaluation of the model representation of convective systems using satellite observations of outgoing longwave radiation. J Geophys Res 115(D20):D20206. https://doi.org/10.1029/2010JD014265

Pearson KJ, Lister GMS, Birch CE, Allan RP, Hogan RJ, Woolnough SJ (2013) Modelling the diurnal cycle of tropical convection across the 'grey zone'. Q J R Meteorol Soc 140(679):491–499. https://doi.org/10.1002/qj.2145

Peng D, Zhou T (2017) Why was the arid and semiarid Northwest China getting wetter in the recent decades? J Geophys Res 122:9060–9075. https://doi.org/10.1002/2016JD026424

Prein AF, Langhans W, Fosser G et al (2015) A review on regional convection-permitting climate modeling: demonstrations, prospects, and challenges. Rev Geophys 53(2):323–361. https://doi.org/10.1002/2014RG000475

Prein AF, Liu C, Ikeda K, Bullock R, Rasmussen RM, Holland GJ, Clark M (2017a) Simulating North American mesoscale convective systems with a convection-permitting climate model. Clim Dyn. https://doi.org/10.1007/s00382-017-3993-2

Prein AF, Rasmussen RM, Ikeda K, Liu C, Clark MP, Holland GJ (2017b) The future intensification of hourly precipitation extremes. Nat Clim Change 7(1):48. https://doi.org/10.1038/NCLIMATE3168

Prein AF, Liu C, Ikeda K, Trier SB, Rasmussen RM, Holland GJ, Clark MP (2017c) Increased rainfall volume from future convective storms in the US. Nat Clim Change 7(12):880. https://doi.org/10.1038/s41558-017-0007-7

Pu B, Cook KH (2012) Role of the West African westerly jet in Sahel rainfall variations. J Clim 25(8):2880–2896. https://doi.org/10.1175/JCLI-D-11-00394.1

Sato T, Miura H, Satoh M, Takayabu YN, Wang Y (2009) Diurnal cycle of precipitation in the tropics simulated in a global cloud-resolving model. J Clim 22(18):4809–4826. https://doi.org/10.1175/2009JCLI2890.1

Seager R, Naik N, Vecchi GA (2010) Thermodynamic and dynamic mechanisms for large-scale changes in the hydrological cycle in response to global warming. J Clim 23(17):4651–4668. https://doi.org/10.1175/2010JCLI3655.1

Shapiro A, Fedorovich E, Rahimi S (2016) A unified theory for the Great Plains nocturnal low-level jet. J Atmos Sci 73(8):3037–3057. https://doi.org/10.1175/JAS-D-15-0307.1

Stein THM, Parker DJ, Hogan RJ, Birch CE, Holloway CE, Lister GMS, Marsham JH, Woolnough SJ (2015) The representation of the West African monsoon vertical cloud structure in the Met Office Unified Model: an evaluation with CloudSat. Q J R Meteorol Soc 141(693):3312–3324. https://doi.org/10.1002/qj.2614

Stephens GL, L'Ecuyer T, Forbes R, Gettlemen A, Golaz JC, Bodas-Salcedo A, Suzuki K, Gabriel P, Haynes J (2010) Dreary state of precipitation in global models. J Geophys Res 115:D24211. https://doi.org/10.1029/2010JD014532

Sun X, Xue M, Brotzge J, McPherson RA, Hu XM, Yang XQ (2016) An evaluation of dynamical downscaling of Central Plains summer precipitation using a WRF-based regional climate model at a convection permitting 4 km resolution. J Geophys Res 121(23):13801–13825. https://doi.org/10.1002/2016JD024796

Trenberth KE, Guillemot CJ (1995) Evaluation of the global atmospheric moisture budget as seen from analyses. J Clim 8(9):2255–2272. https://doi.org/10.1175/1520-0442(1995)008<2255:EOTGAM>2.0.CO;2

Walters D, Boutle I, Brooks M et al (2017) The Met Office unified model global atmosphere 6.0/6.1 and JULES global land 6.0/6.1 configurations. Geosci Model Dev 10(4):1487. https://doi.org/10.5194/gmd-10-1487-2017

Wang CC, Chen GTJ, Carbone RE (2004) A climatology of warm-season cloud patterns over East Asia based on GMS infrared brightness temperature observations. Mon Weather Rev 132(7):1606–1629

Wang CC, Chen GTJ, Huang HL, Carbone RE, Chang SW (2012) Synoptic conditions associated with propagating and nonpropagating cloud/rainfall episodes during the warm season over the East Asian continent. Mon Weather Rev 140(3):721–747

Weisman ML, Skamarock WC, Klemp JB (1997) The resolution dependence of explicitly modeled convective systems. Mon Weather Rev 125(4): 527–548. https://doi.org/10.1175/1520-0493(1997)125<0527:TRDOEM>2.0.CO;2

Yang GY, Slingo J (2001) The diurnal cycle in the tropics. Mon Weather Rev 129(4): 784–801. https://doi.org/10.1175/1520-0493(2001)129<0784:TDCITT>2.0.CO;2

Yu R, Li J (2016) Regional characteristics of diurnal peak phases of precipitation over contiguous China. Acta Meteorol Sin 74(1):18–30. https://doi.org/10.11676/qxxb2016.011 (in Chinese with English abstract)

Yu R, Wang B, Zhou T (2004) Climate effects of the deep continental stratus clouds generated by the Tibetan Plateau. J Clim 17(13): 2702–2713. https://doi.org/10.1175/1520-0442(2004)017<2702:CEOTDC>2.0.CO;2

Yu R, Xu Y, Zhou T, Li J (2007a) Relation between rainfall duration and diurnal variation in the warm season precipitation over central eastern China. Geophys Res Lett 34(13):L13703. https://doi.org/10.1029/2007GL030315

Yu R, Zhou TJ, Xiong A, Zhu Y, Li J (2007b) Diurnal variations of summer precipitation over contiguous China. Geophys Res Lett 34(1):L01704. https://doi.org/10.1029/2006GL028129

Yu R, Li J, Chen H (2009) Diurnal variation of surface wind over central eastern China. Clim Dyn 33(7–8):1089–1097. https://doi.org/10.1007/s00382-008-0478-3

Yuan W, Yu R, Chen H, Li J, Zhang M (2010) Sub-seasonal characteristics of diurnal variation in summer monsoon rainfall over central eastern China. J Clim 23(24):6684–6695. https://doi.org/10.1175/2010JCLI3805.1

Yuan W, Yu R, Zhang M, Lin W, Chen H, Li J (2012) Regimes of diurnal variation of summer rainfall over subtropical East Asia. J Clim 25(9):3307–3320. https://doi.org/10.1175/JCLI-D-11-00288.1

Yuan W, Yu R, Zhang M, Lin W, Li J, Fu Y (2013) Diurnal cycle of summer precipitation over subtropical East Asia in CAM5. J Clim 26(10):3159–3172. https://doi.org/10.1175/JCLI-D-12-00119.1

Zhang Y, Chen H (2016) Comparing CAM5 and super parameterized CAM5 simulations of summer precipitation characteristics over continental East Asia: mean state, frequency-intensity relationship, diurnal cycle, and influencing factors. J Clim 29(3):1067–1089. https://doi.org/10.1175/JCLI-D-15-0342.1

Zhang Q, Zhao Y, Fan S (2016) Development of hourly precipitation datasets for national meteorological stations in China. Torrential Rain Disasters 35(2):182–186. (in Chinese with an English abstract)

Zhou T, Yu R (2005) Atmospheric water vapor transport associated with typical anomalous summer rainfall patterns in China. J Geophys Res 110:D08104. https://doi.org/10.1029/2004JD005413

Zhou T, Yu R, Chen H, Dai A, Pan Y (2008) Summer precipitation frequency, intensity, and diurnal cycle over China: a comparison of satellite data with rain gauge observations. J Clim 21(16):3997–4010. https://doi.org/10.1175/2008JCLI2028.1

Zhu K, Xue M, Zhou B, Zhao K, Sun Z, Fu P, Zheng Y, Zhang X, Meng Q (2018) Evaluation of real-time convection-permitting precipitation forecasts in China during the 2013–2014 summer season. J Geophys Res 123(2):1037–1064. https://doi.org/10.1002/2017JD027445